Precambrian Research 399 (2023) 107223

Contents lists available at ScienceDirect

Precambrian Research

journal homepage: www.elsevier.com/locate/precamres

A c. 1900 Ma Tethyan-type ophiolite in the Penokean Orogen, Pembine, Wisconsin (USA): Insights from the volcanic stratigraphy

George L. Guice [a,b,c,d,*], Daniel R. Viete [d], Robert M. Holder [e], Supratik Roy [d]

[a] Department of Physics, Astronomy and Geosciences, Towson University, 8000 York Road, Towson, MD 21252, USA
[b] Department of Earth and Planetary Sciences, American Museum of Natural History, 200 Central Park West, New York City, NY 10024, USA
[c] Department of Mineral Sciences, Smithsonian National Museum of Natural History, 10th St., and Constitution Ave., Washington, D.C. 20056, USA
[d] Department of Earth & Planetary Sciences, Johns Hopkins University, 3400 N Charles Street, Baltimore, MD 21218, USA
[e] Department of Earth & Environmental Sciences, University of Michigan, 1100 N University Avenue, Ann Arbor, MI 48109, USA

ARTICLE INFO

Keywords:
Boninite
Plate tectonics
Secular change
Suprasubduction zone
SSZ ophiolite

ABSTRACT

Orogenic ophiolites are a hallmark of Phanerozoic plate tectonics, containing igneous lithologies that provide constraints on fundamental tectono-magmatic processes. The c. 1900Ma Pembine Ophiolite (Wisconsin, USA) is associated with the Penokean Orogen and represents a rare example of a proposed Paleoproterozoic ophiolite. The Penokean Orogen shares broad characteristics with Phanerozoic (<541 Ma) orogens, but the origin of the Pembine Ophiolite remains unclear, with the mafic volcanic rocks interpreted as representing either an intra-oceanic arc or continental back arc setting. To test these hypotheses, we present the results of petrography, bulk-rock geochemistry and mineral chemistry for a suite of 34 Pembine rocks, as well as U-Pb zircon geochronology for two samples. Based on trace elements established as immobile in the studied rocks, we demonstrate that mafic volcanism progressed (up-stratigraphic-section) from mid-ocean ridge-like to boninitic. The chemical evolution is identical to that observed in < 250 Ma ophiolites in the Himalayan–Alpine Orogen, which record forearc spreading during the nascent stages of subduction in the Tethys Ocean. We interpret the Pembine Ophiolite as forearc lithosphere formed during subduction initiation and obducted to the margin of the Superior Craton during the Penokean Orogeny. The processes responsible for forming (and preserving) this example of a Paleoproterozoic ophiolite may not have been dissimilar to those operating on the Phanerozoic Earth.

1. Introduction

Orogenic ophiolites — fragments of oceanic crust and upper mantle preserved within continental collision zones (Steinmann et al., 1927) — are a hallmark of Phanerozoic plate tectonics (Dewey and Bird, 1971), with hundreds of examples recognized globally (e.g., Dilek and Furnes, 2014; Stern, 2020). The chemical and isotopic signatures of the mantle portions of ophiolites record processes of melt extraction and metasomatism (e.g., Martin et al., 2016; O'Driscoll et al., 2015; Pagé et al., 2009). In addition, the chemistry of the mafic volcanic stratigraphy — forming the upper part of the crustal portion — records evolution in melting processes (and their tectonic drivers) leading to volcanism (Stern et al., 2012; Whattam and Stern, 2011), including decompression melting during seafloor spreading and flux melting of the mantle wedge during subduction. In comparison to the Phanerozoic ophiolite record, unambiguous Precambrian ophiolites are rare (Moores, 2002; Stern, 2020). Tracking the record of volcanism recorded in ophiolites through geologic time presents opportunities to understand secular change in plate tectonics on Earth, including how oceanic lithosphere was formed and preserved.

The c. 1900 Ma Pembine Ophiolite is an example of a proposed Paleoproterozoic ophiolite (Holm et al., 2020b; Schulz and Cannon, 2007). Other, similarly-aged (c. 2000–1850 Ma) ophiolites from Laurussia include: Jormua in Finland (Kontinen, 1987; Peltonen et al., 1996); Flin Flon in Manitoba (Babechuk and Kamber, 2011; Stern et al., 1995); West Greenland (Garde and Hollis, 2010); and Purtuniq in Quebec (Scott et al., 1999, 1992). The Pembine Ophiolite forms an important part of the Pembine–Wausau Terrane, which was accreted to the southern margin of the Superior Craton along the Niagara Fault (Fig. 1) during the c. 1880–1820 Ma Penokean Orogeny (Schulz and Cannon, 2007; Zi

* Corresponding author.
E-mail address: gguice@towson.edu (G.L. Guice).

https://doi.org/10.1016/j.precamres.2023.107223
Received 19 July 2023; Received in revised form 27 October 2023; Accepted 30 October 2023

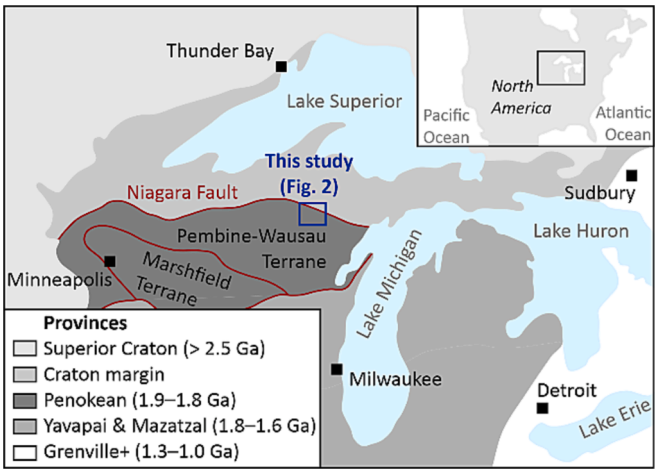

Fig. 1. Simplified geologic map of the Great Lakes region detailing the location and geologic context of the Pembine Ophiolite study area (redrawn after Karlstrom et al., 2001; Zi et al., 2022). Inset: location of Great Lakes region within North America.

et al., 2022). Although the Penokean Orogeny is generally accepted as sharing features with Phanerozoic orogenic belts (Hoffman, 1987; Van Schmus, 1976), the specific nature of its evolution — including the origin of the Pembine–Wausau Terrane — remains a matter of considerable debate (e.g., Schulz and Cannon, 2007; Zi et al., 2022). One outstanding question is whether the Pembine Ophiolite formed as an intra-oceanic arc (e.g., Schulz and Cannon, 2007), a continental back-arc (e.g., Van Wyck and Johnson, 1997; Zi et al., 2022), or via some alternative mechanism. A complicating factor is that the primary mineralogy and chemistry of the Pembine Ophiolite has been overprinted and obscured by multiple phases of Paleoproterozoic deformation and metamorphism, including during the Penokean (geon 18), Yapavai (geon 17), Mazatzal (geon 16) and possibly Baraboo (geon 14) Orogenies (Daniel et al., 2013; Holm et al., 2020b, 1998, 2007, 2005; Medaris et al., 2021; Schulz and Cannon, 2007).

In this paper, our principal aim is to test these hypotheses and establish the primary geochemical affinity and tectonic setting of mafic volcanic rocks of the Paleoproterozoic Pembine Ophiolite, with a secondary aim of adding geochronological constraints to our understanding of the Penokean Orogeny. We present the results of petrography, bulk-rock and mineral geochemistry for a suite of 34 samples, with additional U-Pb zircon geochronology for two samples. We examine the chemical effects of metamorphism/hydrothermal alteration and discuss the suitability of several traditional bulk-rock tectonic discrimination schemes, before assessing the primary chemical signatures recorded by the mafic volcanic rocks. These data are placed in a temporal context using previously published and new U-Pb zircon dates to constrain the tectonic processes responsible for the evolution of the Penokean Orogeny, as well as the nature of Paleoproterozoic plate tectonics globally.

2. The Paleoproterozoic Penokean Orogeny

The tectonic processes recorded by the c. 1880–1820 Ma Penokean Orogeny (Blackwelder, 1914) are considered broadly comparable to those recorded by modern orogenic belts (Hoffman, 1987; Van Schmus, 1976), representing subduction and accretion along the southern margin of the Superior Craton (Schulz and Cannon, 2007; Sims et al., 1989; Zi et al., 2022). Rocks affected include metamorphic rocks of the Archean Superior Craton and associated supracrustal suites, in addition to *meta*-igneous rocks of the Pembine–Wausau and Marshfield Terranes (collectively the Wisconsin Magmatic Terranes), which are interpreted as having been accreted to the Superior Craton along the south-dipping Niagara Fault (Fig. 1; Drenth et al., 2021; Schulz and Cannon, 2007; Van Wyck and Johnson, 1997; Zi et al., 2022). The rocks of the Penokean Orogen also experienced regional metamorphism and deformation during the 1780–1750 Ma Yavapai and 1650–1600 Ma Mazatzal events, and contact metamorphism during intrusion of the c. 1476–1470 Ma Wolf River Batholith (Holm et al., 1998, 2020a, 2005, 2007; Schulz and Cannon, 2007).

The Pembine-Wausau Terrane, which is located south of the Niagara Fault and includes the Pembine Ophiolite, comprises a sequence of volcanic rocks that host c. 1890–1760 Ma (predominantly felsic) intrusive rocks (Sims et al., 1989). The volcanic rocks range from mafic to felsic and show tholeiitic to calc-alkaline compositions (Sims et al., 1989), whereas the felsic intrusive lithologies are predominantly granodiorite and tonalite, with minor diorite and granite (Schulz and Cannon, 2007; Zi et al., 2022). The intermediate–felsic intrusions include three temporal groupings (Fig. 2): (1) the 1889 ± 6 Ma Twelve Foot Falls Diorite (Holm et al., 2020a); (2) a c. 1860 Ma (Sims et al., 1992) or c. 1845 Ma (Zi et al., 2022) suite that includes the Dunbar Gneiss, Marinette Quartz Diorite and Newingham Tonalite; and (3) several Yavapai (1800–1750 Ma) granitic bodies (Holm et al., 2005; Sims, 1992).

The Twelve Foot Falls Quartz Diorite is mapped as intrusive into the basaltic–andesitic Quinnesec Formation and neighboring intermediate–felsic volcanics — the Beecher, Pemene and McAllister Formations of Jenkins (1973), which we group together as the Beecher Formation (Fig. 2) — and interpreted to represent a subvolcanic intrusion cogenetic with the Beecher Formation (Sims and Schulz, 1993; Schulz, 2018). However, a recent 1842 ± 7 Ma U-Pb zircon date for the Beecher Formation has been interpreted to suggest that the intermediate–felsic volcanics are younger than the c. 1889 Ma Twelve Foot Falls Diorite and were therefore deposited on or are in fault contact with the plutonic body (Zi et al., 2022). Monazite separated from the Beecher Formation rocks yielded a U-Pb date of 1775 ± 25 Ma interpreted to record regional metamorphism during the Yavapai event (Zi et al., 2022).

The Marshfield terrane comprises 50 % Archean gneiss and 50 % volcano-sedimentary rocks. The latter includes c. 1870–1860 Ma mafic–felsic volcanic rocks, accompanied by subordinate siliciclastic and minor carbonate sedimentary rocks (Schulz and Cannon, 2007 and references therein). These lithologies are cross-cut by felsic plutonic rocks that yield crystallization ages ranging c. 1890–1840 Ma (Sims et al., 1989). Isotopic studies highlight differences in Pb isotopic signatures of the Superior Craton and the Archean rocks of the Marshfield Terrane, suggesting the latter evolved as a distinct, allochthonous terrane rather than representing a rifted fragment of the former, although the latter hypothesis is not ruled out (Van Wyck and Johnson, 1997).

Questions remain regarding the relationship between the Marshfield and Pembine–Wausau Terranes. Based on lithological and structural characteristics, the Marshfield Terrane has generally been considered a distinct terrane accreted — from the south (current coordinates) — to the Superior Craton margin between 1860 and 1850 Ma, following the accretion of the oceanic Pembine–Wausau Terrane at c. 1875 Ma (Schulz and Cannon, 2007; Sims et al., 1989). Van Wyck and Johnson (1997) argued that the presence of a 2.61 Ga tonalite gneiss in the northern part of the Pembine–Wausau Terrane provides evidence that these two Paleoproterozoic crustal fragments record a common magmatic history, representing distinct domains within a single terrane (Zi et al., 2022). In the latter scenario, the Pembine–Wausau Terrane is considered to have an origin as a continental back-arc (Zi et al., 2022), rather than an intra-oceanic arc (Sims et al., 1989).

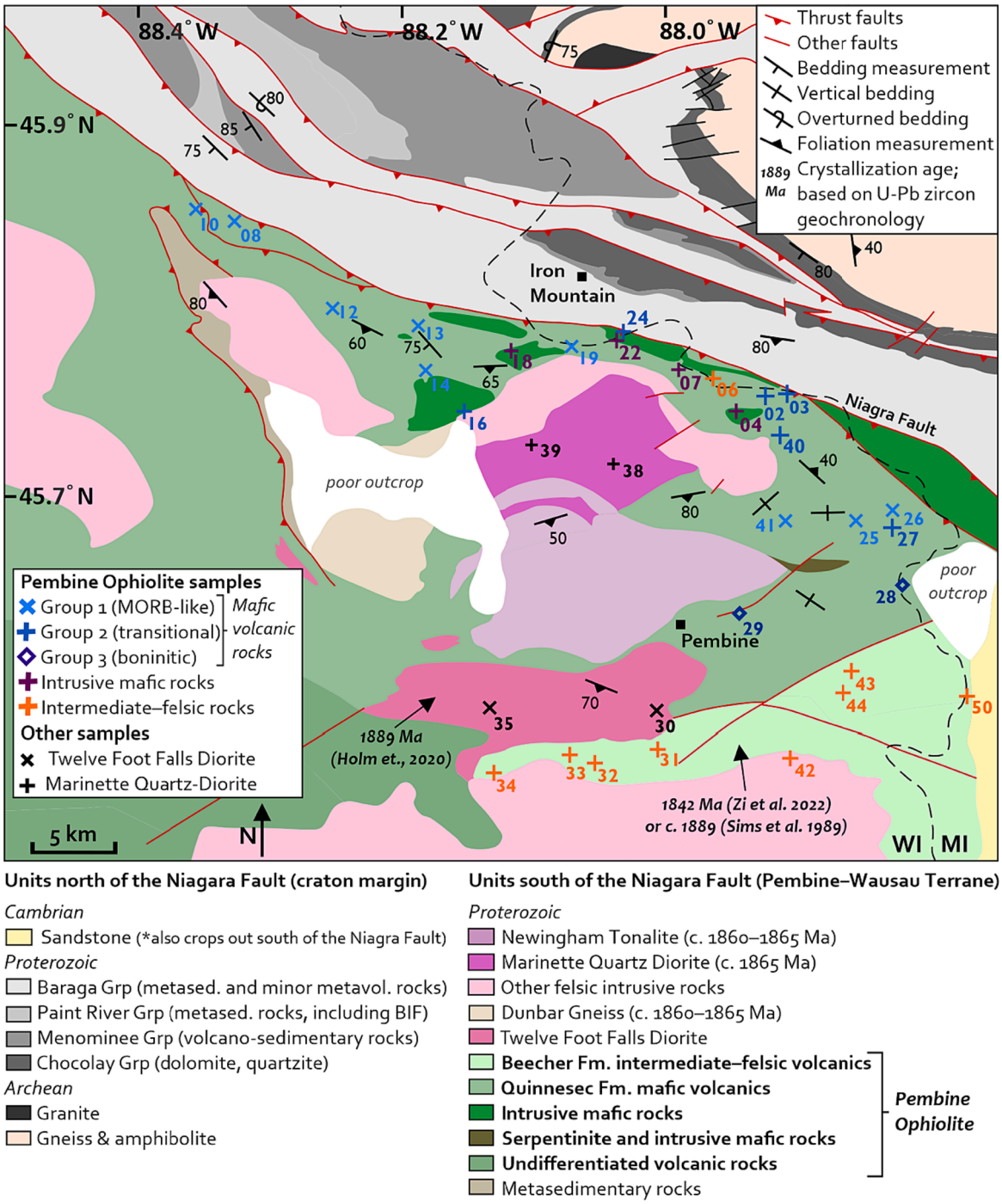

Fig. 2. Geologic map of northeast Wisconsin and northwest Michigan detailing the variety and distribution of samples collected as part of this study (redrawn after Sims and Schulz, 1993).

3. Ophiolite samples studied

3.1. Samples and sample preparation

A total of 34 samples were collected from the eastern part of the Pembine–Wausau Terrane, including 17 samples of mafic volcanic rock (Quinnesec Formation), four samples of intrusive mafic rock, nine samples of intermediate–felsic volcanic rock (eight from the Beecher Formation), two samples of the Marinette Quartz Diorite and two samples of the Twelve Foot Falls Diorite (Fig. 2; Table 1). All samples were collected from a metavolcanic sequence previously interpreted to represent the uppermost parts of a suprasubduction zone (SSZ) ophiolite (Schulz and LaBerge, 2003; Schulz and Cannon, 2007).

Bulk-rock chemical analysis was performed on all samples (Section 4.1), with 16 samples selected for petrographic assessment in thin section, including nine samples of the Quinnesec Formation, four samples of intrusive mafic rocks, and three samples of the Beecher Formation. Major element mineral chemistry was characterized for four mafic samples, with the goal of understanding mineralogical controls on the bulk-rock major element data (see Section 5.1). Two zircon-bearing samples were selected for U-Pb geochronology (Fig. 2): (1) UP19-04, an unnamed gabbro hosted within the Quinnesec Formation in the northern part of the Pembine–Wausau terrane; and (2) UP19-38, a sample of the intrusive Marinette Quartz Diorite. These samples were

Table 1
Sample locations (in decimal degrees) for this study, alongside the analysis type(s) conducted on each sample. Abbreviations: pet = petrography; BR chem = bulk-rock chemistry; Min chem = mineral chemistry; U-Pb zirc = U-Pb zircon geochronology.

Sample	Unit	Latitude	Longitude	Pet	BR chem	Min chem	U-Pb zirc
UP19-02	Quinnesec Formation (mafic volanic rocks)	45.75216	−87.91494	X	X		
UP19-03	Quinnesec Formation (mafic volanic rocks)	45.74894	−87.92657	X	X		
UP19-04	Intrusive mafic rocks	45.74725	−87.94872	X	X		X
UP19-06	Quinnesec Formation (intermediate rock)	45.76057	−87.96948	X	X		
UP19-07	Intrusive mafic rocks	45.76717	−87.99258	X	X	X	
UP19-08	Quinnesec Formation (mafic volanic rocks)	45.84770	−88.33157		X		
UP19-10	Quinnesec Formation (mafic volanic rocks)	45.85342	−88.35971		X		
UP19-12	Quinnesec Formation (mafic volanic rocks)	45.79974	−88.25700		X		
UP19-13	Quinnesec Formation (mafic volanic rocks)	45.79275	−88.19263	X	X		
UP19-14	Quinnesec Formation (mafic volanic rocks)	45.76782	−88.18765		X		
UP19-16	Quinnesec Formation (mafic volanic rocks)	45.75241	−88.15078	X	X	X	
UP19-18	Intrusive mafic rocks	45.77814	−88.12070	X	X	X	
UP19-19	Quinnesec Formation (mafic volanic rocks)	45.78104	−88.07622		X		
UP19-22	Intrusive mafic rocks	45.78545	−88.04353		X		
UP19-24	Quinnesec Formation (mafic volanic rocks)	45.78999	−88.03852	X	X		
UP19-25	Quinnesec Formation (mafic volanic rocks)	45.68933	−87.85870		X		
UP19-26	Quinnesec Formation (mafic volanic rocks)	45.69281	−87.83435		X		
UP19-27	Quinnesec Formation (mafic volanic rocks)	45.68576	−87.83372	X	X		
UP19-28	Quinnesec Formation (mafic volanic rocks)	45.65560	−87.82474	X	X		
UP19-29	Quinnesec Formation (mafic volanic rocks)	45.64070	−87.94621		X		
UP19-30	Twelve Foot Falls Diorite	45.58551	−88.01230		X		
UP19-31	Beecher Formation (int-fel volcanic rocks)	45.56780	−88.01115	X	X		
UP19-32	Beecher Formation (int-fel volcanic rocks)	45.55806	−88.05861		X		
UP19-33	Beecher Formation (int-fel volcanic rocks)	45.56296	−88.07549		X		
UP19-34	Beecher Formation (int-fel volcanic rocks)	45.55651	−88.13316		X		
UP19-35	Twelve Foot Falls Diorite	45.58771	−88.13902		X		
UP19-38	Marinette Quartz-Diorite	45.71736	−88.04295		X		X
UP19-39	Marinette Quartz-Diorite	45.72793	−88.10143		X		
UP19-40	Quinnesec Formation (mafic volanic rocks)	45.73391	−87.91553	X	X		
UP19-41	Quinnesec Formation (mafic volanic rocks)	45.68908	−87.91389	X	X	X	
UP19-42	Beecher Formation (int-fel volcanic rocks)	45.56402	−87.90949	X	X		
UP19-43	Beecher Formation (int-fel volcanic rocks)	45.60366	−87.86429		X		
UP19-44	Beecher Formation (int-fel volcanic rocks)	45.59375	−87.87062		X		
UP19-50	Beecher Formation (int-fel volcanic rocks)	45.59401	−87.77684	X	X		

chosen to supplement recently published U-Pb geochronology on the Beecher Formation, Dunbar Gneiss, Newingham Tonalite and Twelve Foot Falls Diorite (Holm et al., 2020; Zi et al., 2022). See Table 1 for sample locations and the analyses types conducted on each sample.

3.2. Petrographic summary

The mafic volcanic rocks of the Quinnesec Formation (n = 9 of 17) contain 15–80 modal % amphibole (variably altered to fine-grained chlorite) and 20–85 modal % plagioclase (variably altered to sericite), with accessory ilmenite, epidote, quartz, apatite, titanite, calcite, magnetite and pyrite. The mean grain size of samples is 0.3–1.0 mm (Fig. 3). Polyphase, sub-millimetre-scale veins containing quartz, chlorite, pyrite and calcite locally cross-cut some samples in places.

The intrusive mafic rocks (n = 3 of 4) are mineralogically comparable to the mafic volcanic rocks of the Quinnesec Formation, containing: 30–75 modal % amphibole (variably altered to fine-grained chlorite) and 25–70 modal % plagioclase (variably altered to sericite), with accessory quartz, calcite, titanite, ilmenite, apatite, magnetite and pyrite. Mean grain sizes are 1.5–2 mm, with sub-millimeter- to millimeter-scale veins containing quartz, pyrite, calcite and chlorite.

The intermediate–felsic volcanic rocks of the Beecher Formation (n = 2 of 8) contain 5–15 modal % plagioclase (+/- amphibole and quartz) phenocrysts and 85–95 modal % microcrystaline groundmass. The nature of the phenocrysts is variable; plagioclase ranges from subhedral to euhedral in some samples to rounded, < 3.5 mm-diameter, highly altered patches in others. Rare hornblende phenocrysts occur as subhedral, < 1.5 mm grains showing thick rims of fine-grained (<300 μm) amphibole. The microcrystalline groundmass is composed of fine-grained (<200 μm) aggregates of quartz, plagioclase, amphibole and minor mica.

4. Methods

4.1. Bulk-rock geochemistry

Following the removal of weathered surfaces using a rock saw, samples were crushed and powdered in alumina/ceramic for bulk-rock geochemical analysis. Glass discs were prepared by mixing 1 g of sample with 4 g of Li tetraborate, and major element analysis was conducted using a Malvern PANanlytical Inc. Xetium X-Ray fluorescence spectrometer in the Franklin & Marshall X-Ray Laboratory, Franklin & Marshall College. Trace element analysis was performed on the same glass discs by laser ablation inductively coupled plasma mass spectrometry (LA-ICP-MS) using a Teledyne Cetac Analyte G2 193 nm laser, equipped with a HelEx II two-volume cell, coupled to an Agilent 8900 triple quadrupole ICP-MS in the TeMPO Laboratory, Johns Hopkins University (JHU). Data were collected using 600 μm linescans, employing a scan rate of 10 μm/s, laser repetition rate of 20 Hz, fluence of 3 J cm^{-2} and a square spot with side length of 100 μm. Helium was introduced into the cell at a rate of 0.35 L min^{-1} and ablation cup at a rate of 0.25 L min^{-1}, and Ar makeup gas was added at a rate of 0.8 L min^{-1} prior to introduction of the analyte stream to the ICP–MS. All unknowns were run in duplicate, with the second analysis used to verify results from the first. Standard references glasses NIST612, NIST610, AGV-2G and BHVO-2G were each measured once for every six unknowns, with NIST612 used as the primary standard for data reduction and NIST610, AGV-2G and BHVO-2G used as secondary–quaternary standards. Measured average abundance for each element in each of the secondary standards were within 15 % of values reported on the GeoReM database (Jochum et al., 2005).

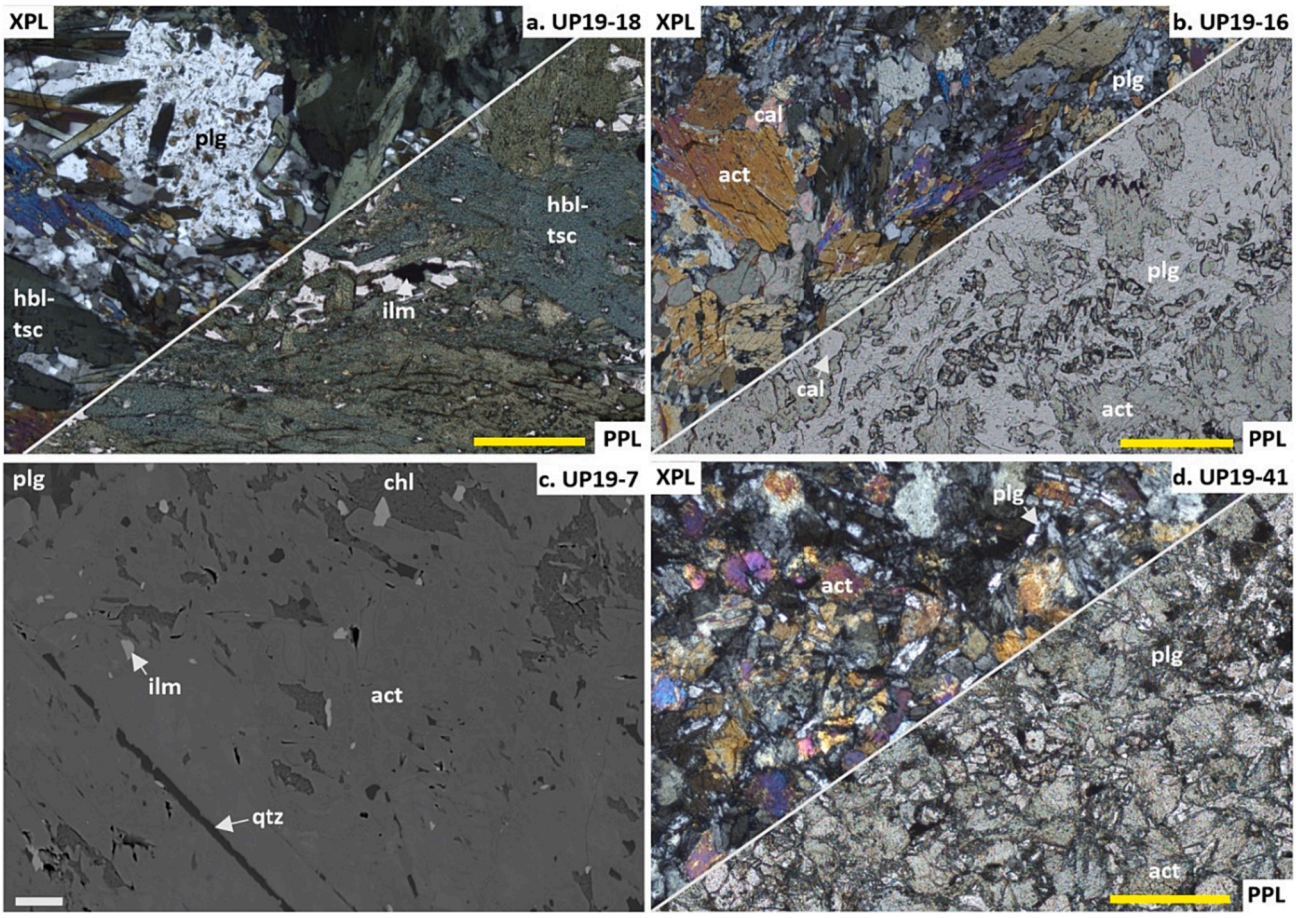

Fig. 3. Photomicrographs (a, b, d) and back-scattered electron (BSE) images (c) illustrating the range of metamorphic minerals and textures observed in the Pembine Ophiolite rocks subject to chemical characterization using electron microprobe analysis. Note the presence of hornblende–tschermakite series amphiboles in UP19-18 (a), whereas actinolite dominates all other samples shown (b–d). The significance of these observations — in the context of the metamorphic evolution of the Pembine Ophioloite — is discussed in Section 5.1.1. White scale bar = 20 μm; yellow scale bar = 500 μm. Abbreviations: act = actinolite; cal = calcite; chl = chlorite; hbl-tch = hornblende–tschermakite series; ilm = ilmenite; qtz = quartz; plg = plagioclase.

4.2. Major element mineral chemistry

Quantitative mineral analyses were conducted in the Department of Mineral Sciences, Smithsonian National Museum of Natural History, using a JEOL 8900 electron microprobe equipped with five wavelength dispersive spectrometers (WDS) and one energy dispersive spectrometer (EDS). Spot analyses used a 1 μm diameter spot, 15 kV accelerating voltage and 20nA beam current. A total of 220 quantitative spot analyses were performed on silicate mineral phases, including 87 on amphibole grains, 21 on chlorite grains, 39 on epidote grains and 73 on plagioclase grains. The full dataset is available, in element oxide wt. % format, in the supplementary material.

Primary standardization was conducted using a suite of Smithsonian standard reference materials, with secondary standards — pyrope (NMNH143968), garnet (NMNH87375), Cr-augite (NMNH164905), chromite (NMNH118075), manganite (USNM157872), ilmenite (USNM96189) and hornblende (NMNH143965) — analyzed regularly to monitor accuracy and precision of the analyses (see supplementary material). The average abundance of elements analyzed for the standards were within 1.5 % of certified values, with precision ranging from 0.4 to 2.8 % RSD.

4.3. U-Pb zircon geochronology

Geochronology samples were crushed using a stainless-steel ring-and-puck mill, sieved to < 250 μm then washed to remove clay-sized particles. The sieved and washed material was subjected to magnetic separation using a Frantz LB-1 separator. The highly non-magnetic fraction was subjected to density separation using diiodomethane (specific gravity = 3.32 g cm^{-3}). Zircon grains were picked from the diiodomethane-heavy fraction on the basis of optical properties, annealed at 900 °C for 66 h and mounted in 1″ epoxy rounds. Rounds were polished to a 0.3 μm grit size, carbon coated and imaged using a Deben Centaurus cathodoluminescence (CL) detector attached to a Thermo Scientific Helios G4 UC scanning electron microscope (SEM) in the Materials Characterization & Processing Facility, JHU.

Mounted and CL-imaged zircon grains were analyzed using the previously mentioned LA-ICP-MS in the TeMPO Laboratory, JHU. Spot analyses were conducted using a square spot with a diameter of 40 x 40 μm, 250 (UP19-04) or 200 (UP19-38) shots at a laser repetition rate of 10 Hz (UP19-04) or 8 Hz (UP19-38) and fluence of 1.33 J cm^{-2} (UP19-04) or 3 J cm^{-2} (UP19-38). Helium was introduced into the cell at a rate of 0.35 L min^{-1} (UP19-04) or 0.5 L min^{-1} (UP19-38) and ablation cup at a rate of 0.325 L min^{-1} (UP19-04) or 0.3 L min^{-1} (UP19-38), and Ar makeup gas was added at a rate of 0.8 L min^{-1} prior to introduction of the analyte stream to the ICP–MS. 'SQUID' tubing used to smoothen the signal at the detector. Data were collected over three analytical sessions in June 2022, and May and June 2023.

Zircon standard reference materials 91,500 (1063.6 ± 0.3 Ma: Schoene et al., 2006; Wiedenbeck et al., 1995), Plešovice (337.13 ± 0.37 Ma: Sláma et al., 2008), Temora 2 (416.78 ± 0.33 Ma: Black et al., 2004), and FC-1 (1099.9 ± 1.1 Ma: Paces and Miller Jr, 1993) were

measured prior to every analytical run and every six unknown analyses. Standard reference material 91,500 was the primary standard material used for data reduction, which was conducted in Iolite v4 (Paton et al., 2011), employing a median fit to the standard data (autospline fit was used for UP19-04 due to all reference materials analyzed displaying a uniform, monotonic drift in intensity) and using the downhole fractionation application of Paton et al. (2010). Prior to age calculation, a 'lab excess uncertainty' of 2 % was added in quadrature to all isotope ratios outputted from iolite (method outlined in Horstwood et al., 2016). Concordia diagrams were plotted and ages calculated using IsoplotR (Vermeesch, 2018). Full details of standard and unknown analyses (following the reporting guidelines of Horstwood et al., 2016) are provided in the supplementary material, as are statistical parameters demonstrating satisfactory performance of the standards.

5. Results and discussion

5.1. Effects of metamorphism and alteration: Establishing robust geochemical proxies

5.1.1. Major elements

The rocks of the Pembine–Wausau Terrane have been affected by multiple phases of metamorphism (Section 2.0), with the preserved mineral assemblages recording metamorphic grades ranging from upper greenschist to mid-amphibolite facies (Geiger and Guidotti, 1989; Schulz and Cannon, 2007). This variation in metamorphic mineral assemblage is reflected in the amphibole species present in the Pembine Ophiolite mafic rocks assessed in this study. In most samples, the amphibolite species are magnesium-hornblende, actinolite and actinolite-hornblende (greenschist to lower-amphibolite facies), whereas highly pleochroic tschermakite and Fe-tschermakite (mid- to upper-amphibolite facies) occurs in one sample (UP19-18; supplementary material Fig. A).

Plagioclase compositions also vary between samples. Plagioclase in sample UP19-41 – the most easterly sample for which mineral chemical data was collected – shows limited chemical variation, with this sample exhibiting the lowest Al_2O_3 (21–22 wt%) and CaO (0.7–2.4 wt%) contents, but highest SiO_2 (66–69 wt%) and Na_2O (6.3–8.5 wt%) contents (Supplementary Table B). Plagioclase in Sample UP19-18 also shows limited chemical variation and comparable Na_2O (4.6–8.2 wt%) contents to UP19-41, but exhibits slightly higher Al_2O_3 (23–25 wt%) and CaO (4.4–6.9 wt%) contents, as well as lower SiO_2 (60–63 wt%) contents. Plagioclase in UP19-16 and −07 shows broader compositional variation, with Al_2O_3 from 23 − 34 wt%, CaO from 2 − 18 wt%, SiO_2 from 46 − 63 wt% and Na_2O from 1 − 8 wt% (Supplementary Table B).

These mineralogical observations have implications for the major element compositions of the bulk rocks analyzed as part of this study (Fig. 4). The trend from actinolite towards tschermakite amphibole compositions — reflecting the progressive effects of fluid alteration/transport during amphibolite facies metamorphism — has the effect of locally decreasing SiO_2 and MgO contents (Fig. 4a), while also increasing FeO, Al_2O_3 and Na_2O (Supplementary Figure A). The chlorite alteration would have caused (at least locally) SiO_2, CaO and TiO_2 loss and mild MgO gain (Fig. 4), while the variation in plagioclase compositions could reflect a combination of primary crystallization and secondary alteration during metamorphism. The major element compositions of the analyzed bulk-rocks therefore represent a combination of primary igneous processes and metasomatic alteration/transport during metamorphism.

This raises broader questions about the utility of major element discrimination plots for elucidating the chemical affinity and tectonic environment of lavas that have experienced extensive metamorphism, as commonly encountered in orogenic ophiolites. The boninite classification scheme of Pearce and Reagan (2019), which utilizes multiple elements that have been established as fluid-mobile (at least locally) during metamorphism of the Pembine Ophiolite (e.g., SiO_2, MgO), is considered inappropriate for the rocks studied in this paper. On the TiO_2 versus MgO plot (Fig. 4d), five samples plot in the boninite field, but only two samples classify as boninite according to the rigorous trace element analysis presented in Section 5.1.2 (see below). This discrepancy in chemical classification is interpreted as a consequence of Mg mobility during metamorphism. Similarly, other plots commonly used to establish primary chemical affinity would yield unreliable results if applied to the mafic volcanic rocks of the Pembine Ophiolite, including: (1) bivariate plots with MgO on the horizontal axis, commonly used to compare major element compositions among ophiolites and modern tectonic environments (e.g., Dilek et al., 2008; Dilek and Thy, 1998); (2) FeO/MgO ratio (or Mg-number), commonly used to distinguish tholeiitic from calc-alkaline affinity lavas (e.g., Dilek et al., 2008) as well as to differentiate between mid-ocean ridge basalt (MORB), island arc basalt (IAB) and boninite (e.g., Pe-Piper et al., 2004).

In summary, many of the major element proxies appropriately applied to young (<200 Ma), relatively unmetamorphosed ophiolites are not useful for discrimination of magmatic processes and tectonic environments in ancient orogenic belts such as the c. 1880–1820 Ma Penokean Orogeny of North America, which has experienced multiple, widespread episodes of metamorphism and deformation (and associated element mobility).

5.1.2. Trace elements

Determining the correlation between individual trace elements and those considered most immobile at crustal conditions (e.g., Y, Yb, Zr; Cann, 1970; Guice et al., 2018, Guice et al., 2019) can be a useful approach to constraining bulk-rock trace element mobility in co-genetic suites of mafic rocks. This simple method provides no details about which stage of metamorphism was responsible for element mobility, but does broadly indicate the magnitude of metamorphism-related metasomatism. Here, Yb was selected as the most immobile element, based on it having the lowest correlation with Ba (a highly mobile element) and highest correlation with other highly immobile elements (Y, Zr). To avoid complications arising from the effects of crystal fractionation, only the mafic volcanic samples ($n = 17$) were included in linear correlation calculations. Results for fits among trace elements and Yb are shown in supplementary material Figure B.

Linear fits to the trace element bivariate plots for the Pembine mafic volcanic rocks show that abundance of the most compatible elements (Nd–Lu on normalized trace element plots; Fig. 5) correlate strongly with Yb ($R^2 = 0.77$–0.99) and do not correlate at all with Ba ($R^2 < 0.1$). This suggests that these elements were relatively immobile during metamorphism and hydrothermal alteration. In contrast, the most incompatible trace elements (Rb–Sr on the normalized trace element plot; Fig. 5) show poor correlations with Yb ($R^2 < 0.15$), suggesting these elements were likely mobilized relative to Yb during the multiple phases of metamorphism experienced by the Pembine Ophiolite mafic rocks. Only trace elements considered relatively immobile during metamorphism (Nd–Lu on normalized trace element plots; Fig. 5) are here used to establish the primary chemical signatures of the mafic volcanic samples from the Pembine Ophiolite. These data underline the importance of conducting a detailed assessment of element mobility prior to applying bulk-rock trace element data to investigate the primary magmatic affinity of metamorphosed mafic volcanic rocks (Guice, 2019 and references therein).

5.2. Mafic volcanic rock chemistry: A progression from MORB-like to boninitic volcanism

Based on elements considered immobile (Section 5.1), the Quinnesec Formation mafic volcanic rocks analyzed as part of this study are subdivided into three groups (Fig. 5). Groups 1 and 3 are end-members that resemble mid-ocean ridge basalt (MORB) and mean Izu-Bonin-Mariana (IBM) boninite, respectively, whereas Group 2 is transitional between these end-members. All mafic volcanic rocks that were assessed contain

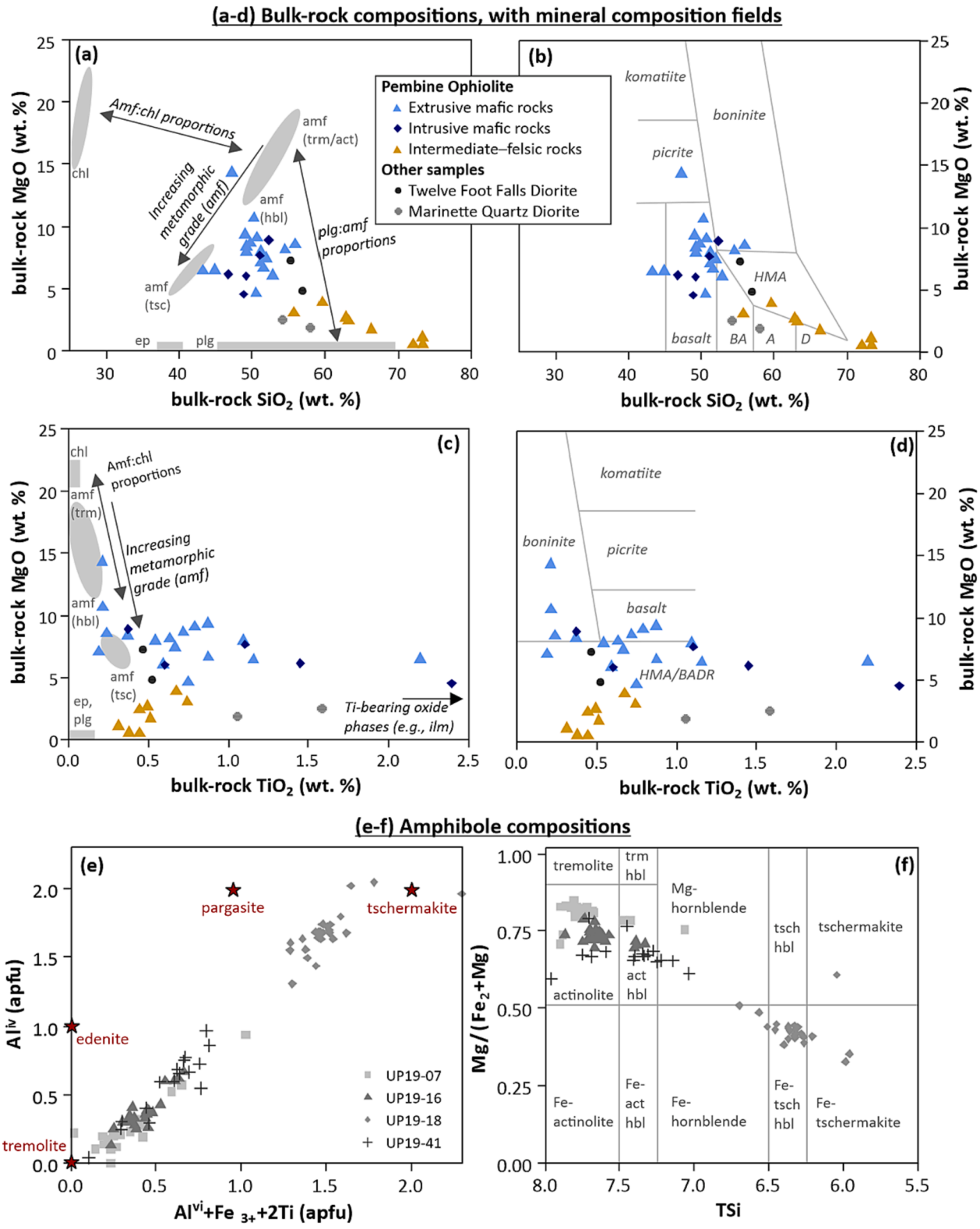

Fig. 4. (a-d) Bulk-rock bivariate plots for rocks analyzed from the Pembine Ophiolite. (a) and (c) detail the mineralogical controls of the bulk-rock composition, including annotations outlining the chemical effects of metamorphism. (b) and (d) are the same plots as (a) and (c), respectively, but instead show the major- and minor-element classification fields of Pearce and Reagan (2019). Abbreviations: A = andesite; amf = amphibolite; BA = basaltic andesite; D = dacite; HMA = high-magnesium andesite; BADR = basalt–andesite–dacite–rhyolite; all other abbreviations as for Fig. 3. (e-f) Amphibole compositions.

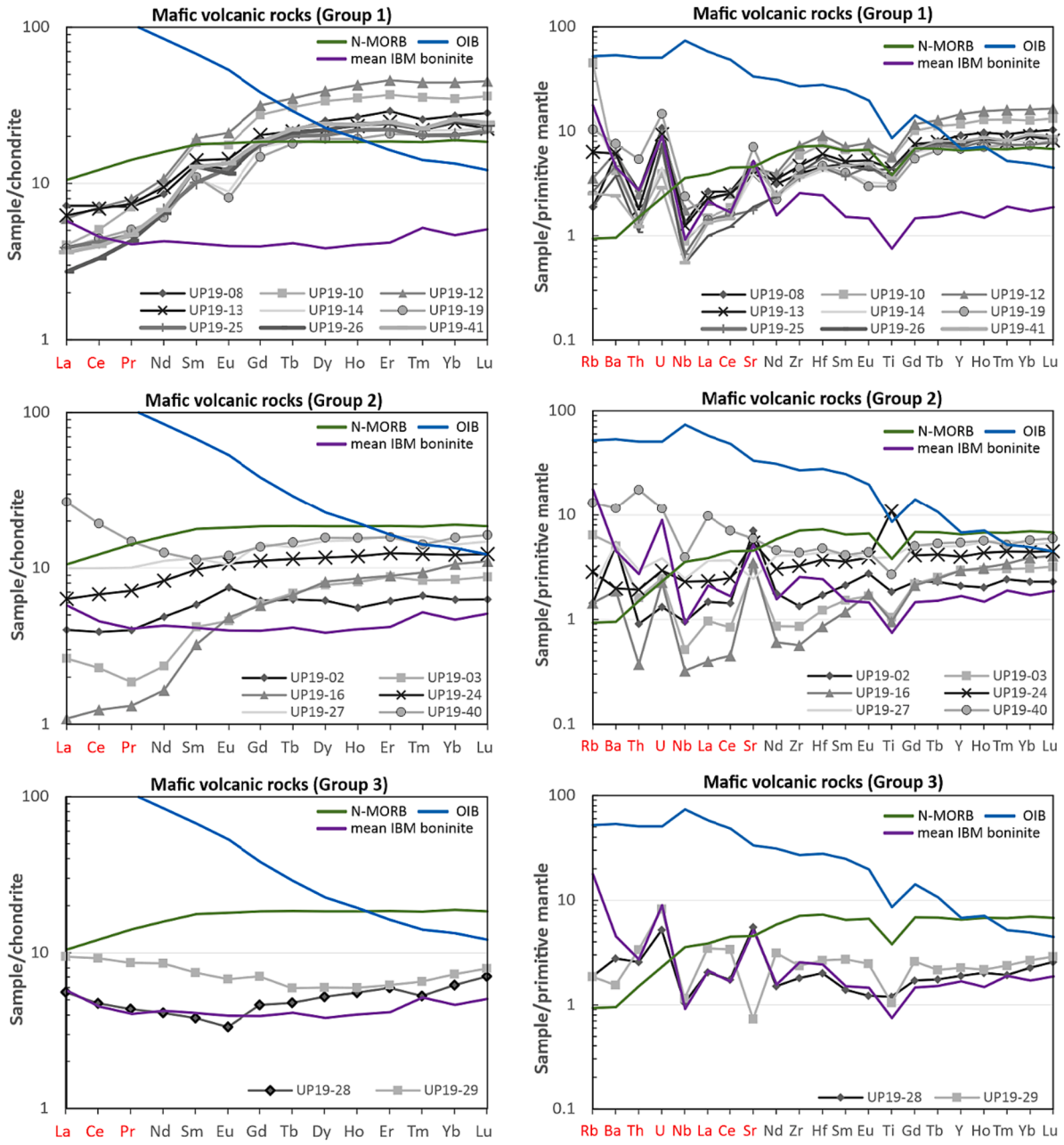

Fig. 5. Chondrite-normalized rare earth element (REE) plots (left column) and primitive mantle-normalized trace element plots (right column) illustrating the trace element compositions of the mafic volcanic rocks from the Pembine Ophiolite. For elements considered relative immobile (in dark grey on the x axis), group 1 compositions resemble N-MORB, while group 3 composition resemble the mean boninite from the Izu-Bonin-Mariana. Normalizing values are from McDonough and Sun (1995); MORB and OIB compositions are from Sun and McDonough (1989); mean Izu-Bonin-Mariana (IBM) boninite composition calculated using data downloaded from the GEOROC database (https://georoc.eu/). Red elements are considered mobile in the studied rocks (see Section 5.1.2). The full dataset are included in the supplementary material.

5–14 wt% MgO, 43–56 wt% SiO_2 and 13–15 wt% Al_2O_3, and have mineral assemblages described in Section 3.1.

The immobile trace element characteristics of the three groups are as follows (Fig. 5): Group 1 (MORB-like; n = 9) samples are enriched in compatible elements ($[Lu]_{pmN}$ = 7.8–16.5), with positively sloping trace-element patterns ($[Zr/Lu]_{pmN}$ = 0.4–0.6), mild positive Zr–Hf anomalies and mild negative Ti anomalies (Fig. 5); Group 2 (transitional; n = 6) samples are depleted in compatible trace elements relative to Group 1 ($[Lu]_{pmN}$ = 2.3–5.9), exhibiting positively sloping to near-flat trace element patterns ($[Zr/Lu]_{pmN}$ = 0.1–0.8) and mild negative Zr and Ti anomalies; Group 3 (boninite-like; n = 2) samples are strongly depleted in compatible trace elements relative to Group 1 ($[Lu]_{pmN}$ = 2.6–2.9) and show near-flat trace element patterns ($[Zr/Lu]_{pmN}$ = 0.7–0.8).

Group 1 and Group 2 samples are spatially concentrated close to the Niagara Fault, in the north of the mapped Quinnesec Formation (Figs. 1, 2), whereas the Group 3 samples occur closer to the contact with the intermediate–felsic volcanic rocks (Beecher Formation), at the southern extent of the Quinnesec Formation. Thus, assuming the intermediate–felsic volcanic rocks represent the stratigraphic top of the Pembine Ophiolite (Sims et al., 1989), the described geochemical evolution from Group 1 (MORB-like) to Group 3 (boninite-like) occurs in an up-stratigraphic direction (Fig. 6). Based on a sub-vertical dip, the maximum stratigraphic thickness for the mafic volcanic rocks is

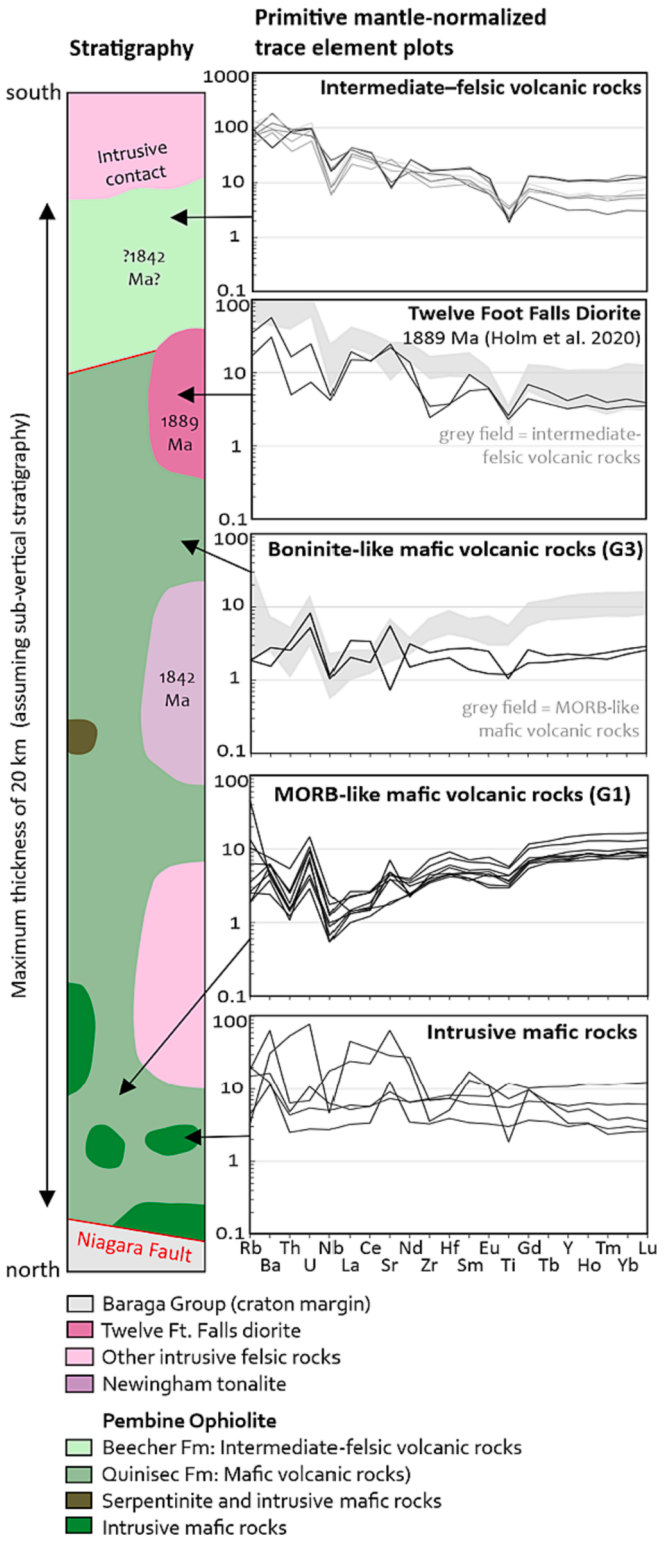

Fig. 6. Stratigraphic column detailing the stratigraphy of the Pembine Ophiolite, with a specific focus on the chemostratigraphic evolution of the mafic volcanic rocks, as described in Section 5.2. Normalizing values from McDonough and Sun (1995). Abbreviations: MORB = mid-ocean ridge basalt. "G1" and "G3" refer to the Group 1 and 3 mafic volcanics, respectively, as defined in Section 5.2 and Fig. 5.

approximately 18 km; however, the true thickness is almost certainly significantly less (Fig. 6) and will depend on the true dip of the Quinnesec Formation, which is unclear based on current geologic mapping (Fig. 2). LaBerge et al. (2003) suggest the Quinnesec may be several km thick and that the Beecher Formation (our usage, combining the Beecher, Pemene and McAllister Formations of Jenkins, 1973) may also be several km thick.

5.3. Temporal constraints on the evolution of the Pembine Ophiolite

5.3.1. Existing temporal constraints

5.3.1.1. Pre-Penokean (>1880 Ma) magmatism. The history of magmatism associated with the Pembine Ophiolite started with eruption of the MORB-like units of the Quinnesec Formation, which are close to the stratigraphic base (see Section 5.2; Fig. 6). These rocks are constrained as older than c. 1890 Ma by a U-Pb zircon age for the Twelve Foot Falls Diorite (1889 ± 6 Ma: Holm et al., 2020). However, the only geochronology work directly dating these rocks is a whole-rock Sm–Nd date of 1870 ± 56 Ma for the Quinnisec Formation (Beck and Murthy, xxxx), which is not precise enough to differentiate it from other units of the Pembine–Wausau Terrane. The Twelve Foot Falls Diorite has an εNd (1900 Ma) value of + 4.54 (Schulz and Ayuso, 1998), consistent with a (single-stage) depleted mantle extraction timing identical to its crystallization age (c. 1889 Ma: Holm et al., 2020) and similar to the Nd composition of the Quinnesec Formation (Beck and Murthy, 1991). Primary crystallization of the Beecher Formation was recently dated at 1842 ± 7 Ma (U-Pb zircon; Zi et al., 2022), challenging interpretations of the Beecher Formation as cogenetic with the geochemically-similar Twelve Foot Falls Diorite (Sims, 1992).

5.3.1.2. Penokean-age (1880–1820 Ma) magmatism. Intrusive igneous units dated to the 1880–1820 Ma interval include the Marinette Quartz Diorite, Newingham Tonalite and Spike Horn Creek Granite, which are all interpreted — based on field relationships — to post-date the Dunbar Gneiss (Sims, 1992). Sims et al. (1992) dated the Dunbar Gneiss, Marinette Quartz Diorite and Newingham Tonalite at 1862 ± 5 Ma, 1857 ± 16 Ma and 1861 ± 40 Ma, respectively (all by U-Pb zircon). Zi et al. (2022) recently published younger U-Pb zircon dates of 1845 ± 7 Ma for the Dunbar Gneiss and 1847 ± 10 Ma for the Newingham Tonalite. Neodymium isotope analyses for the Dunbar Gneiss, Marinette Quartz Diorite, Hoskin Lake Granite and Newingham Tonalite suggest these units crystallized from evolved magmas (Van Wyck and Johnson, 1997; Schulz and Ayuso, 1998).

5.3.1.3. Yavapai-age (1800–1750 Ma) metamorphism. The Pembine Ophiolite experienced metamorphism at c. 1775, constrained by a U-Pb monazite date from the intermediate–felsic volcanic rocks of the Beecher Formation (Zi et al., 2022). This recently published monazite date is associated with the Yavapai metamorphic event recorded in continental terranes north of the Niagara Fault (Holm et al., 2007; Schneider et al., 2004) and farther south in Wisconsin (Medaris et al., 2021).

5.3.2. New U-Pb zircon constraints

To better constrain the timing of magmatism in the Pembine Ophiolite, samples of a gabbro within the Quinnesec Formation (UP19-04) and of the Marinette Quartz Diorite (UP19-38) were dated by U-Pb zircon LA-ICP-MS. Full data tables for the geochronology work are provided in the supplementary material.

Sample UP19-04 — a mafic unit with SiO_2 = 46.75 wt% — yielded four zircons. They are translucent-brown and euhedral, with aspect ratios of ~ 2:1 and a short-dimension width of ~ 100 μm. The zircons display oscillatory zoning in CL (Fig. 7C) and have Th/U values of 1.1–1.9, which is suggestive of igneous origin. Individual grains were large enough to fit 3–4 spots on each, for a total of 14 analyses. Analyses

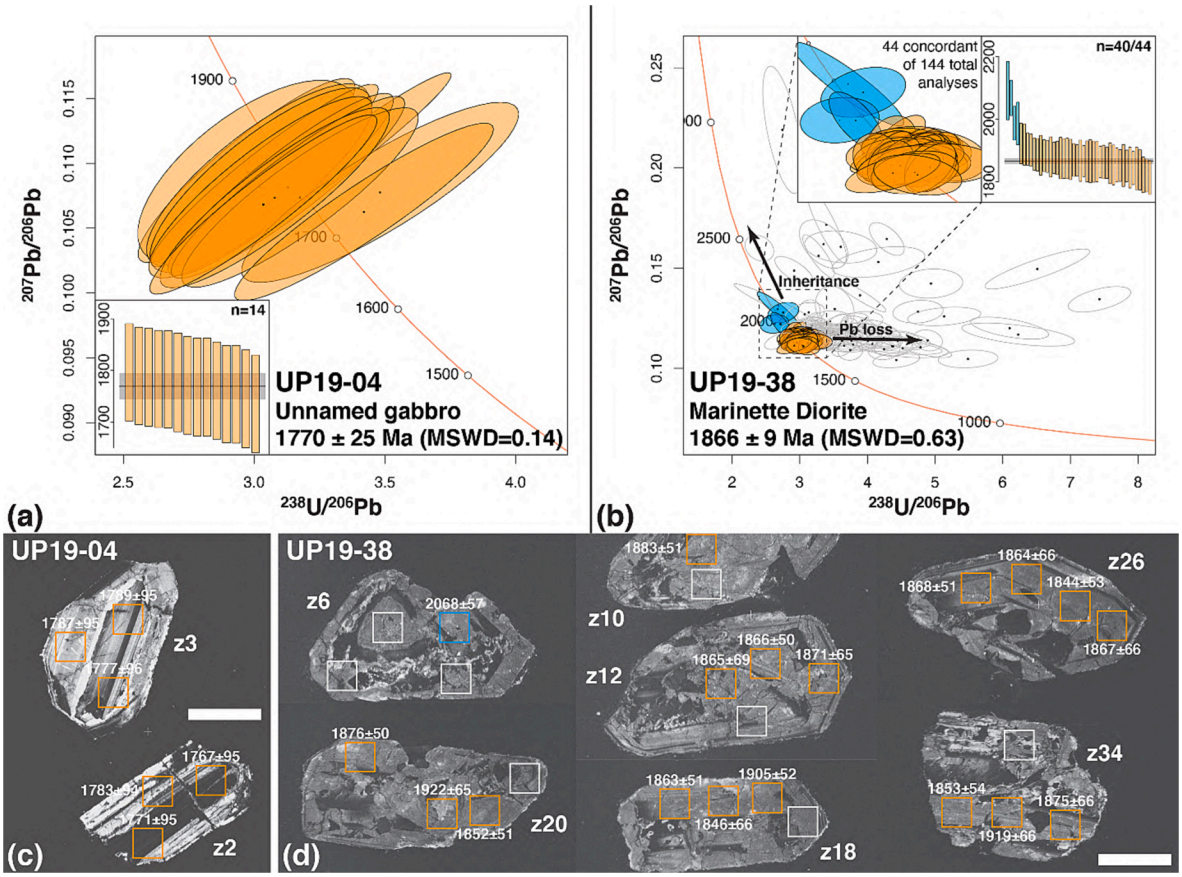

Fig. 7. U-Pb zircon geochronology results for this study. (a) Tera-Wasserburg concordia plot showing all analyses for the UP19-04 sample of unnamed gabbro, with inset showing weighted mean plot. (b) Tera-Wasserburg concordia plot showing all analyses for the UP19-38 sample of Marinette Quartz Diorite, with blow up of main data cluster and inset showing weighted mean plot. Individual analyses were filtered for a 2.5 % discordance cutoff: discordant data are colorless; concordant but anomalously old data are cyan; concordant main-population data are orange. (c) CL images for representative set of zircons from UP19-04, showing locations of individual analyses and their dates. (d) CL images for a representative set of zircons from UP19-38, showing locations of individual analyses and their dates. Orange, cyan and white color code as for sub-figure (b). MSWD = mean squared weighted deviation. All dates are $^{207}Pb/^{206}Pb$ dates, with 2se uncertainty.

clustered on concordia, yielding a $^{207}Pb/^{206}Pb$ date of 1770 ± 25 Ma (MSWD = 0.14, n = 14; Fig. 7A) that we interpret to date crystallization during the Yavapai event. The gabbro bodies within the Quinnesec Formation are isotropic (unlike the heavily-deformed Quinnesec Formation metavolcanics that host them), which is consistent with a late-tectonic or post-tectonic intrusive timing.

Marinette Quartz Diorite sample UP19-38 yielded numerous, heavily metamict zircons that are opaque-chocolate brown. The grains are euhedral, displaying well-developed terminations, aspect ratios between 1:1 and 5:1, and a short-dimension width of 100–200 μm. The zircons are relatively uniform in CL response, displaying oscillatory zoning at the rims but incoherent zoning in the cores, suggestive of extensive metamictization (Fig. 7d). Grains have Th/U values of 0.1–2.3. Four analyses were performed on 36 different zircons, for a total of 144 analyses. The Tera-Wasserburg plot of the data shows evidence of both Pb loss associated with metamictization and minor inheritance (Fig. 7b). Applying discordance filters of 1 %, 2.5 % and 5 % — based on $^{206}Pb/^{238}U$ date vs. $^{207}Pb/^{235}U$ date, using the $^{238}U/^{235}U$ ratio of Hiess et al. (2012) — resulted in culling of the original dataset (n = 144) to n = 23, n = 44 and n = 72, respectively. The two most aggressive culling approaches yielded single statistical age populations with indistinguishable $^{207}Pb/^{206}Pb$ dates of 1867 ± 12 Ma (MSWD = 0.8, n = 40; 1 % cutoff) and 1866 ± 9 Ma (MSWD = 0.63, n = 40; 2.5 % discordance cutoff) when old outliers are excluded. We choose to report the date obtained using the 2.5 % cutoff (Fig. 7b).

Our c. 1770 Ma date for the undeformed, Quinnesec-hosted gabbro sample (UP19-04) suggests that the gabbro intrusions within the Quinnesec Formation are associated with the Yavapai event; though previous interpretations have considered these gabbros to be cogenetic with the Quinnesec Formation (e.g., Sims et al., 1992), it appears that they significantly post-date that volcanism. The Yavapai event has also been associated with widespread regional metamorphism in the Pembine–Wausau Terrane (Zi et al., 2022) and the marginal (Superior) terranes to the north (Holm et al., 2007; Schneider et al., 2004) and Yavapai terrane to the south (Medaris et al., 2021). The enriched MORB-like compositions of these gabbros (Fig. 6) suggest that the Yavapai event may have involved decompression melting and advection of heat from the mantle into the crust, raising interesting questions of heat sources for the Yavapai regional metamorphism.

Our 1866 ± 9 Ma date for the Marinette Quartz Diorite is slightly older than the 1845 ± 7 Ma date Zi et al. (2022) recently determined for the Dunbar Gneiss, which the Marinette Quartz Diorite intrudes; however, the difference between these dates (~1 %) is within the generally accepted accuracy for in-situ U-Pb geochronology (e.g., Košler et al., 2013). On the other hand, the 1842 ± 7 Ma date for the Beecher Formation (Zi et al., 2022) is ~ 2.5 % younger than the 1889 ± 6 Ma date for the Twelve Foot Falls Diorite (Holm et al., 2020), whichis interpreted to have intruded the Beecher Formation (Sims, 1992). Given apparent widespread perturbation to U-Pb zircon systematics in the Beecher Formation and Dunbar Gneiss by younger Yavapai metamorphism (Zi et al., 2022), we argue that the Zi et al. (2022) dates should be treated as minima. If the Beecher Formation is older than (or cogenetic with) the Twelve Foot Falls Diorite then the volume of pre-Penokean (>1880 Ma) volcanism can be extended significantly. Additional dating of the

Beecher Formation and overlying volcanics and/or Nd analysis of these units (i.e., testing for juvenile vs. more evolved origin) may help to shed light on this issue.

5.4. *The Pembine Ophiolite: Forearc oceanic lithosphere produced during subduction initiation*

In previous tectonic models for the Paleoproterozoic Penokean Orogeny, the Pembine Ophiolite has been interpreted as: (1) a c. 1900 Ma intra-oceanic arc that was accreted to the southern margin of the Superior Craton at c. 1875 Ma (Schulz and Cannon, 2007); or (2) a continental back-arc (Van Wyck and Johnson, 1997), with ultramafic–mafic magmatism a product of back arc extension and decompression melting at c. 1845 Ma (Zi et al., 2022). In the intra-oceanic arc model, the Pembine–Wausau Terrane is interpreted as a suprasubduction zone ophiolite, with the accretion of this terrane at c. 1875 Ma marking the culmination of south-dipping subduction (current coordinates), triggering subduction polarity flip and back-arc extension (Schulz and Cannon, 2007). By contrast, the continental back arc model proposes that the Pembine Ophiolite was associated with West Pacific-style 'tectonically-switching' accretionary orogenesis, which involved pulses of extension and contraction (see Collins, 2002) over a north-dipping subduction zone (Zi et al., 2022). The data presented here supports the suprasubduction zone ophiolite model of Schulz and Cannon (2007), with the Pembine Ophiolite further interpreted here as having formed in response to forearc spreading during subduction initiation at or before 1890 Ma.

The geochemical evolution recorded in the Quinnesec Formation mafic volcanics — from MORB-like at the base (n = 9) to boninitic (n = 2) at higher stratigraphic levels (see Section 5.2) — is a characteristic feature of < 250 Ma SSZ ophiolites; ophiolites showing this volcanic evolution include many "Tethyan-type" ophiolites of the Alpine–Himalayan mountain system (Dilek and Furnes, 2014). Although geochemical and stratigraphic variability occurs among examples, these Tethyan ophiolites show a consistent trend towards boninite-like compositions stratigraphically upward. As summarized in Fig. 8, this geochemical progression is characterized by decreases in the abundance of: (1) the most compatible trace elements (e.g., Yb, Lu; Fig. 8a–b); (2) the high field strength elements (HFSE; e.g., Zr and Ti; Fig. 8c); and (3) moderately compatible trace elements (e.g., Nd; Fig. 8d). Notably, in the Nd v. Yb plot (Fig. 8d the Pembine rocks define two arrays — one consistent with the Mirdita, Oman and Pindos data, the other consistent with the Troodos data — reflecting the geochemical diversity among mafic volcanic stratigraphies of Tethyan ophiolites. The stratigraphic top of the Pembine Ophiolite comprises intermediate–felsic volcanic rocks with distinctive negative Nb–Zr–Hf–Ti anomalies (Fig. 6), which is a feature that is also characteristic of Tethyan ophiolites (Dilek et al., 2008). The striking geochemical and lithological similarities between

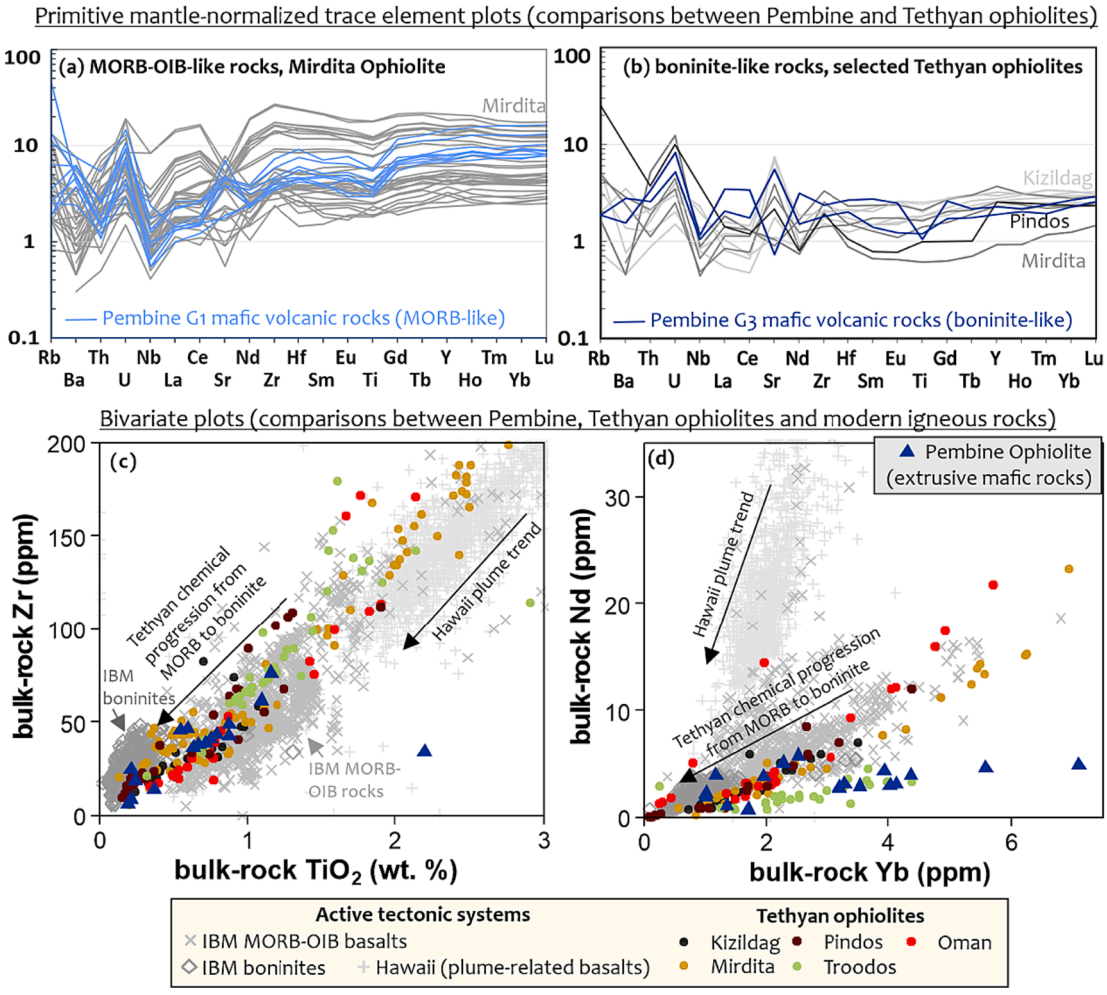

Fig. 8. Primitive mantle-normalized trace element plots (a–b) and trace element bivariate plots (c–d) showing the similarity of the mafic volcanic rocks of the Pembine Ophiolite to MORB (G1–Pembine) and boninite (G3–Pembine) samples from various Tethyan ophiolites. Plume-related basalts from Hawaii are also included on the bivariate plots for comparison, with the Pembine data distinct from these plume compositions. Tethyan data from: Dilek et al. (2008); Dilek and Thy (2009); Pe-Piper et al. (2004); Saccani and Photiades (2004). IBM and Hawaii data from the GEOROC database (https://georoc.eu/).

the Pembine Ophiolite and Tethyan ophiolites raises the intriguing possibility that the processes of magmagenesis (e.g., mantle source, melting trigger and degree of partial melting) and the typical evolution of these processes at c. 1900 Ma were similar to those operative in the Mesozoic and Cenozoic Eras.

There is growing consensus that Tethyan ophiolites preserve young, buoyant forearc lithosphere ideally situated for obduction following subduction initiation (Casey and Dewey, 1984; Wakabayashi and Dilek, 2004). This hypothesis has been strengthened by petrologic and geochemical findings for the IBM forearc, which is associated with active subduction in the West Pacific, southeast of Japan (Ishizuka et al., 2006, 2011). The mafic volcanic rocks of the IBM forearc show the same up-stratigraphic-section geochemical progression as the Tethyan ophiolites (Dilek and Furnes, 2009), recording evolution from tholeiitic lavas associated with extension and forearc seafloor spreading to calc-alkaline and arc lavas reflecting the increasing influence of subduction-derived fluids (Whattam and Stern, 2011; Stern et al., 2012).

Our observation that the mafic volcanic chemical stratigraphy of the Pembine Ophiolite is comparable to that of Mesozoic, Tethyan ophiolites raises the possibility that it formed as forearc oceanic lithosphere — comparable to that of the modern IBM — during subduction initiation at c. 1900 Ma, and was subsequently obducted onto the Superior Craton. This interpretation requires that the Pembine Ophiolite is an oceanic-derived terrane.

5.5. *Paleoproterozoic ophiolites and the evolution of plate tectonics on Earth*

Secular change and the evolution of Earth's tectonic mode is a topic of considerable debate. Some authors argue that plate tectonic-like processes have operated consistently since 3500 Ma or earlier (Ackerson et al., 2021; Furnes et al., 2009), while others suggest that modern plate tectonic processes may only have been localized and/or ephemeral until c. 1000 Ma (Hamilton, 2003; Stern, 2005, 2020). However, the majority of researchers place the onset of plate tectonics somewhere between 3000 and 2500 Ma (e.g., Cawood et al., 2018), with this interpretation supported by the temporal evolution of several metamorphic (Brown and Johnson, 2018; Holder et al., 2019; Holder and Viete, 2023), bulk-rock geochemical (Johnson et al., 2019; Tang et al., 2016), mineral chemical (Ackerson et al., 2021), and isotopic (e.g., Dhuime et al., 2015) proxies. The proposed existence of Archean ophiolites — including the 2510 Ma Dongwanzi-Zunhua complex in the North China Craton (Kusky et al., 2001), the 2530 Ma Devanur complex in the Dharwar Craton (Yellappa et al., 2012), the 3500 Ma Jamestown (De Wit et al., 1987) and 3500 Ma Muldersdrif–Modderfontein complexes in the Kaapvaal Craton (Anhaeusser, 2006), and the 3800 Ma Isua Greenstone Belt in the North Atlantic Craton (Furnes et al., 2007) — have also been cited as evidence supporting the operation of plate tectonics before 2500 Ma. However, it should be noted that not all of Archean ophiolite interpretations are widely accepted (e.g., Kamber 2015).

Whether an ephemeral Paleoproterozoic process or one that had been operating for hundreds of millions or billions of years prior to 1.9 Ga, the geologic record preserves strong evidence that plate tectonics operated during the time interval represented by the Penokean Orogeny (Stern, 2023). Metamorphic rocks recording relatively low thermobaric ratios — suggestive of formation in subduction zones — occur in the 2.1–1.8 Ga interval (e.g., Brown and Johnson, 2018, 2019; Holder and Viete, 2023), and a cluster of ophiolites are also recognized at this time interval (Section 1.0; Condie, 2018; Stern, 2023). What remains unresolved, however, is how the tectonic, magmatic and metamorphic processes operational during the 2.1–1.8 Ga interval compare to those occurring on Earth today. Has plate tectonics operated consistently since before 2 Ga, or have Earth's major plate tectonic processes and their petrologic products changed in character over this time interval?

As described above, the MORB-like to boninitic volcanic progression recorded in the Pembine Ophiolite (and Tethyan ophiolites) is considered to record decompression melting and seafloor spreading associated with local extension during subduction initiation, followed by increasing influence of slab-derived fluids, leading to the traditional arc signature (Kelemen et al., 1993). The HFSE anomalies that characterize this late chemical signature are interpreted as associated with rutile-present melting of depleted upper mantle, with this mineral retaining HFSE in the source region (Klemme et al., 2005). The chemical similarity of the Pembine Ophiolite's mafic volcanic stratigraphy to Tethyan ophiolites and the IBM arc (Section 5.4) implies that the processes forming oceanic lithosphere at c. 1900 Ma may have been similar to processes active in subduction zones today (Reagan et al., 2017).

One potential caveat to this hypothesis is the relative lack of ultramafic rocks in the Pembine Ophiolite. These lithologies typically dominate the lowermost portions of complete or near-complete Tethyan-type ophiolites and form the diagnostic mantle portion (Fig. 9). According to current mapping, ultramafic rocks in the Pembine Ophiolite are restricted to an area less than 4 km x 1 km that is coincident with the middle of the ophiolite stratigraphy (Fig. 2; Fig. 6). Though the best-preserved examples of Tethyan ophiolites contain large swathes of ultramafic rock (Fig. 9), many dismembered/heavily tectonized Phanerozoic ophiolites are dominated by mafic rocks (e.g., Becker et al., 2023). In these cases, the lack of ultramafic rocks may be attributed to tectonic processes during obduction/later faulting, rather than representing a fundamental difference in the processes forming the ophiolitic lithosphere. As described in Section 2.0, the Pembine Ophiolite has experienced multiple phases of tectonism since its formation at c. 1900 Ma. As the contact between the mafic and ultramafic-dominated portions of ophiolites represents a rheological boundary along which faults are likely to localize, detachment and segregation of the mafic from ultramafic portions should not be unexpected. The apparent lack of other classic ophiolite features, including pelagic sediments and a well-developed sheeted dyke complex (with plagiogranites), could also be attributed to the multiple episodes of tectonism experienced by the Pembine rocks.

6. Conclusions

1. The Pembine Ophiolite is a fragment of oceanic lithosphere that was obducted to the southern margin of the Superior Craton during the Paleoproterozoic Penokean Orogeny. The ophiolite stratigraphy is < 18 km thick and preserves (from stratigraphic base): mafic volcanic rocks, containing intrusive mafic rocks that are concentrated mostly towards the base; and extrusive intermediate–felsic volcanic rocks. The stratigraphic base of the ophiolite is bound by the Niagara Fault, while the stratigraphic top is in direct contact with felsic intrusive rocks.

2. Major elements commonly used in bulk-rock geochemical discrimination diagrams (e.g., Si, Mg) — including the popular classification scheme of Pearce and Reagan (2019) — were mobilized during the amphibolite- and greenschist-facies metamorphism of the Pembine Ophiolite volcanics, making them unreliable tectonomagmatic proxies here.

3. Relatively immobile trace element compositions of the Quinnesec Formation mafic volcanic rocks record an up-stratigraphic-section geochemical progression from MORB-like to boninitic in the Pembine Ophiolite. This geochemical evolution is identical to that observed for < 250 Ma Tethyan ophiolites preserved in the Alpine–Himalayan system.

4. Our new U-Pb zircon geochronology conducted on an intrusive mafic rock (UP19-04) is suggestive of mafic magmatism at c. 1770 Ma, during the Yavapai orogenic event and potentially via decompression melting. Other new U-Pb zircon geochronology — conducted on the Marinette Quartz Diorite — suggests that this unit crystallized at c. 1866 Ma.

5. The Pembine Ophiolite is interpreted as having formed in response to forearc spreading during subduction initiation at c. 1900 Ma. The upper, intermediate–felsic volcanic unit reflects subsequent arc

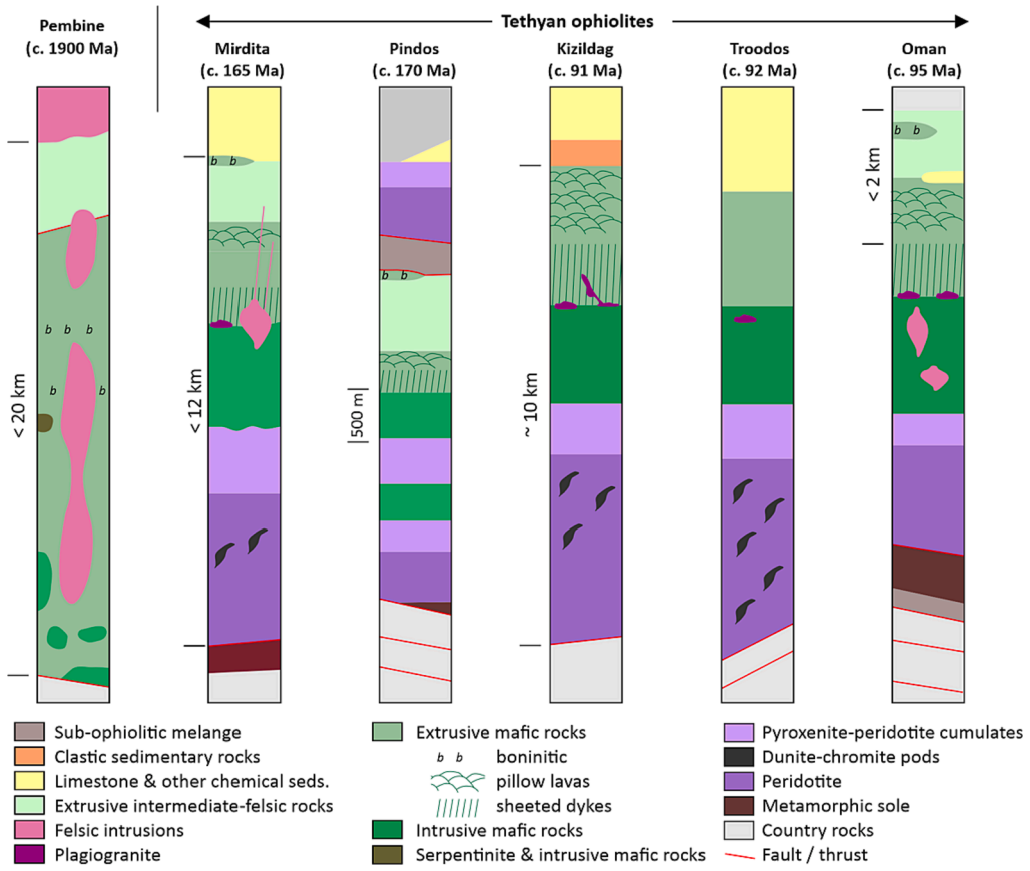

Fig. 9. Comparison between the stratigraphy of the Pembine Ophiolite and those of several Tethyan ophiolites. Tethyan ophiolite stratigraphies redrawn after Dilek and Furnes (2009).

magmatism as the subduction zone matured, with the entire package obducted to the continental margin of the Superior Craton during the Penokean Orogeny (c. 1875 Ma: Schulz & Cannon, 2007) and then affected by regional metamorphism during the Penokean Orogeny (c. 1830 Ma: Holm et al., 2007; Schneider et al., 2004) and the Yavapai event (c. 1775 Ma: (Holm et al., 2007; Schneider et al., 2004; Zi et al., 2022).

6. The chemical similarity of the Pembine Ophiolite mafic volcanic stratigraphy to multiple examples of Tethyan ophiolites (and the modern IBM arc) implies that the Pembine Ophiolite represents a rare ophiolite of Paleoproterozoic age, and that the (plate) tectonic framework at c. 1900 Ma may not have been significantly dissimilar to that of modern Earth.

CRediT authorship contribution statement

George L. Guice: Conceptualization, Data curation, Formal analysis, Investigation, Visualization, Writing – original draft, Writing – review & editing. **Daniel R. Viete:** Conceptualization, Data curation, Formal analysis, Funding acquisition, Investigation, Methodology, Project administration, Supervision, Visualization, Writing – review & editing. **Robert M. Holder:** Conceptualization, Investigation, Validation, Methodology, Writing – review & editing. **Supratik Roy:** Investigation, Data curation, Formal analysis, Methodology, Writing – review & editing.

Declaration of Competing Interest

The authors declare that they have no known competing financial interests or personal relationships that could have appeared to influence the work reported in this paper.

Data availability

All data is included in the supplementary material.

Acknowledgements

Tim Rose, Rob Wardell and Michael Ackerson provided assistance with microprobe work at NMNH. Elyjah Bassford, Dana Brenner, Joseph Browning-Hanson, Antonella Macoretta and Justin Sontag provided assistance with zircon separation, preparation and analysis at JHU. Stanley Mertzman performed the XRF work at Franklin & Marshall College. GLG acknowledges a 2019 Peter Buck Postdoctoral Fellowship awarded by the Smithsonian Institution, and a 2022 Kalbfleisch Postdoctoral Fellowship awarded by the American Museum of Natural History. DRV acknowledges funding from a National Science Foundation (NSF) CAREER Grant (NSF-2042631), JHU Catalyst Grant and Hopkins Extreme Materials Institute Seed Grant, and the Department of Earth & Planetary Sciences, JHU. Trace element geochemistry and U-Pb zircon geochronology work by LA-ICP-MS at JHU was supported by an NSF Infrastructure and Facilities Grant (NSF-1831766). Fieldwork was performed on the traditional lands of the Menominee and Ojibwe Nations. The authors declare no competing interests. We would also like to thank Prof. Victoria Pease for constructive feedback and considerate Editorial Handling, as well as two anonymous reviewers and Gordon Medaris for constructive comments that helped to improve our manuscript.

Appendix A. Supplementary material

Supplementary data to this article can be found online at https://doi.org/10.1016/j.precamres.2023.107223.

References

Ackerson, M.R., Trail, D., Buettner, J., 2021. Emergence of peraluminous crustal magmas and implications for the early Earth. Geochemical Perspect. Lett. 17, 50–54.

Anhaeusser, C.R., 2006. A reevaluation of Archean intracratonic terrane boundaries on the Kaapvaal Craton, South Africa: Collisional suture zones? Geol. Soc. Am. Spec. Pap. 405, 193–210.

Babechuk, M.G., Kamber, B.S., 2011. An estimate of 1.9 Ga mantle depletion using the high-field-strength elements and Nd-Pb isotopes of ocean floor basalts, Flin Flon Belt, Canada. Precambrian Res. 189, 114–139. https://doi.org/10.1016/j.precamres.2011.05.006.

Beck, J.W., Murthy, V.R., 1991. Evidence for continental crustal assimilation in the Hemlock Formation flood basalts of the early Proterozoic Penokean Orogen, Lake Superior region. US Government Printing Office.

Becker, N.A., George, F.R., Guice, G.L., Crowley, J.L., Nelson, W.R., Browning-Hanson, J. F., Roy, S., Viete, D.R., 2023. Subduction initiation recorded in the Dadeville Complex of Alabama Georgia, USA. Geosphere. https://doi.org/10.1130/GES02643.1.

Black, L.P., Kamo, S.L., Allen, C.M., Davis, D.W., Aleinikoff, J.N., Valley, J.W., Mundil, R., Campbell, I.H., Korsch, R.J., Williams, I.S., 2004. Improved 206Pb/238U microprobe geochronology by the monitoring of a trace-element-related matrix effect; SHRIMP, ID–TIMS, ELA–ICP–MS and oxygen isotope documentation for a series of zircon standards. Chem. Geol. 205, 115–140.

Blackwelder, E., 1914. A summary of the orogenic epochs in the geologic history of North America. J. Geol. 22, 633–654.

Brown, M., Johnson, T.E., 2018. Secular change in metamorphism and the onset of global plate tectonics. Am. Mineral. 103, 181–196. https://doi.org/10.2138/am-2018-6166.

Cann, J.R., 1970. Rb, Sr, Y, Zr and Nb in some ocean floor basaltic rocks. Earth Planet. Sci. Lett. 10, 7–11. https://doi.org/10.1016/0012-821X(70)90058-0.

Casey, J.F., Dewey, J.F., 1984. Initiation of subduction zones along transform and accreting plate boundaries, triple-junction evolution, and forearc spreading centres-implications for ophiolitic geology and obduction. Geol. Soc. Spec. Publ. 13, 269–290. https://doi.org/10.1144/GSL.SP.1984.013.01.22.

Cawood, P.A., Hawkesworth, C.J., Pisarevsky, S.A., Dhuime, B., Capitanio, F.A., Nebel, O., 2018. Geological archive of the onset of plate tectonics. Phil. Trans. R. Soc. Lond. 376.

Condie, K.C., 2018. A planet in transition: The onset of plate tectonics on Earth between 3 and 2 Ga? Geosci. Front. 9, 51–60. https://doi.org/10.1016/j.gsf.2016.09.001.

Daniel, C.G., Pfeifer, L.S., Jones III, J. V, McFarlane, C.M., 2013. Detrital zircon evidence for non-Laurentian provenance, Mesoproterozoic (ca. 1490–1450 Ma) deposition and orogenesis in a reconstructed orogenic belt, northern New Mexico, USA: Defining the Picuris orogeny. Bulletin 125, 1423–1441.

De Wit, M.J., Hart, R.A., Hart, R.J., 1987. The Jamestown Ophiolite Complex, Barberton mountain belt: a section through 3.5 Ga oceanic crust. J. African Earth Sci. 6, 681–730. https://doi.org/10.1016/0899-5362(87)90007-8.

Dewey, J.F., Bird, J.M., 1971. Origin and emplacement of the ophiolite suite: Appalachian ophiolites in Newfoundland. J. Geophys. Res. 76, 3179–3206.

Dhuime, B., Wuestefeld, A., Hawkesworth, C.J., 2015. Emergence of modern continental crust about 3 billion years ago. Nat. Geosci. 8, 552–555. https://doi.org/10.1038/NGEO2466.

Dilek, Y., Furnes, H., 2009. Structure and geochemistry of Tethyan ophiolites and their petrogenesis in subduction rollback systems. Lithos 113, 1–20.

Dilek, Y., Furnes, H., 2014. Ophiolites and their origins. Elements 10, 93–100. https://doi.org/10.2113/gselements.10.2.93.

Dilek, Y., Furnes, H., Shallo, M., 2008. Geochemistry of the Jurassic Mirdita Ophiolite (Albania) and the MORB to SSZ evolution of a marginal basin oceanic crust. Lithos 100, 174–209. https://doi.org/10.1016/j.lithos.2007.06.026.

Dilek, Y., Thy, P., 1998. Structure, petrology and seafloor spreading tectonics of the Kizildag Ophiolite, Turkey. Geol. Soc. Spec. Publ. 148, 43–69. https://doi.org/10.1144/GSL.SP.1998.148.01.04.

Dilek, Y., Thy, P., 2009. Island arc tholeiite to boninitic melt evolution of the Cretaceous Kizildag (Turkey) ophiolite: Model for multi-stage early arc-forearc magmatism in Tethyan subduction factories. Lithos 113, 68–87. https://doi.org/10.1016/j.lithos.2009.05.044.

Drenth, B.J., Cannon, W.F., Schulz, K.J., Ayuso, R.A., 2021. Geophysical insights into Paleoproterozoic tectonics along the southern margin of the Superior Province, central Upper Peninsula, Michigan, USA. Precambrian Res. 359, 106205.

Furnes, H., de Wit, M., Staudigel, H., Rosing, M., Muehlenbachs, K., 2007. A vestige of Earth's oldest ophiolite. Science 80, 1704–1707. https://doi.org/10.1126/science.1139170.

Furnes, H., Rosing, M., Dilek, Y., de Wit, M., 2009. Isua supracrustal belt (Greenland)-A vestige of a 3.8 Ga suprasubduction zone ophiolite, and the implications for Archean geology. Lithos 113, 115–132. https://doi.org/10.1016/j.lithos.2009.03.043.

Geiger, C.A., Guidotti, C.V., 1989. Precambrian metamorphism in the southern Lake Superior region and its bearing on crustal evolultion. Geosci. Wisconsin 13, 1–33.

Guice, G.L., 2019. Origin and geodynamic significance of ultramafic-mafic complexes in the North Atlantic and Kaapvaal Cratons. Cardiff University.

Guice, G.L., McDonald, I., Hughes, H.S.R., Schlatter, D.M., Goodenough, K.M., Macdonald, J.M., Faithfull, J.W., 2018. Assessing the validity of negative high field strength-element anomalies as a proxy for Archaean subduction: Evidence from the Ben strome complex. NW Scotland. Geosciences 8, 338. https://doi.org/10.3390/geosciences8090338.

Guice, G.L., McDonald, I., Hughes, H.S.R., Anhaeusser, C.R., 2019. An evaluation of element mobility in the Modderfontein ultramafic complex, Johannesburg: Origin as an Archaean ophiolite fragment or greenstone belt remnant? Lithos 332–333, 99–119. https://doi.org/10.1016/j.lithos.2019.02.013.

Hamilton, W.B., 2003. An alternative earth. GSA Today 13, 4–12. https://doi.org/10.1130/1052-5173(2003)013<0004:AAE>2.0.CO;2.

Hiess, J., Condon, D.J., McLean, N., Noble, S.R., 2012. 238U/235U systematics in terrestrial uranium-bearing minerals. Science 80). 335, 1610–1614.

Hoffman, P.F., 1987. Early Proterozoic foredeeps, foredeep magmatism, and Superior-type iron-formations of the Canadian Shield. Proterozic Lithospheric Evol. 17, 85–98.

Holder, R.M., Viete, D.R., Brown, M., Johnson, T.E., 2019. Metamorphism and the evolution of plate tectonics. Nature 572, 378–381. https://doi.org/10.1038/s41586-019-1462-2.

Holm, D.K., Anderson, R., Boerboom, T.J., Cannon, W.F., Chandler, V., Jirsa, M., Miller, J., Schneider, D.A., Schulz, K.J., Van Schmus, W.R., 2007. Reinterpretation of Paleoproterozoic accretionary boundaries of the north-central United States based on a new aeromagnetic-geologic compilation. Precambrian Res. 157, 71–79.

Holm, D., Schneider, D., Coath, C.D., 1998. Age and deformation of Early Proterozoic quartzites in the southern Lake Superior region: Implications for extent of foreland deformation during final assembly of Laurentia. Geology 26, 907–910.

Holm, D., Medaris, L.G., McDannell, K.T., Schneider, D.A., Schulz, K., Singer, B.S., Jicha, B.R., 2020a. Growth, overprinting, and stabilization of Proterozoic provinces in the southern Lake Superior region. Precambrian Res. 339, 105587 https://doi.org/10.1016/j.precamres.2019.105587.

Holm, D., Medaris, L.G., McDannell, K.T., Schneider, D.A., Schulz, K., Singer, B.S., Jicha, B.R., 2020b. Growth, overprinting, and stabilization of Proterozoic provinces in the southern Lake Superior region. Precambrian Res. 339 https://doi.org/10.1016/j.precamres.2019.105587.

Holm, D.K., Van Schmus, W.R., MacNeill, L.C., Boerboom, T.J., Schweitzer, D., Schneider, D., 2005. U-Pb zircon geochronology of Paleoproterozoic plutons from the northern midcontinent, USA: Evidence for subduction flip and continued convergence after geon 18 Penokean orogenesis. Geol. Soc. Am. Bull. 117, 259–275.

Ishizuka, O., Kimura, J.I., Li, Y.B., Stern, R.J., Reagan, M.K., Taylor, R.N., Ohara, Y., Bloomer, S.H., Ishii, T., Hargrove, U.S., Haraguchi, S., 2006. Early stages in the evolution of Izu-Bonin arc volcanism: New age, chemical, and isotopic constraints. Earth Planet. Sci. Lett. 250, 385–401. https://doi.org/10.1016/j.epsl.2006.08.007.

Ishizuka, O., Tani, K., Reagan, M.K., Kanayama, K., Umino, S., Harigane, Y., Sakamoto, I., Miyajima, Y., Yuasa, M., Dunkley, D.J., 2011. The timescales of subduction initiation and subsequent evolution of an oceanic island arc. Earth Planet. Sci. Lett. 306, 229–240. https://doi.org/10.1016/j.epsl.2011.04.006.

Holder, R.M., Viete, D.R., 2023. The metamorphic rock record through Earth's history. In: Kohn, M.J. (Ed.), Treatise on Geochemistry, third ed. Section 2, The Lithosphere.

Jenkins, R.A., 1973. The geology of the Beecher and Pemene townships, Marinette County, Wisconsin, in: Proceedings,. pp. 15–16.

Jochum, K.P., Nohl, U., Herwig, K., Lammel, E., Stoll, B., Hofmann, A.W., 2005. GeoReM: a new geochemical database for reference materials and isotopic standards. Geostand. Geoanalytical Res. 29, 333–338.

Johnson, T.E., Kirkland, C.L., Gardiner, N.J., Brown, M., Smithies, R.H., Santosh, M., 2019. Secular change in TTG compositions: Implications for the evolution of Archaean geodynamics. Earth Planet. Sci. Lett. 505, 65–75. https://doi.org/10.1016/j.epsl.2018.10.022.

Kelemen, P.B., Shimizu, N., Dunn, T., 1993. Relative depletion of niobium in some arc magmas and the continental crust: partitioning of K, Nb, La and Ce during melt/rock reaction in the upper mantle. Earth Planet. Sci. Lett. 120, 111–134.

Klemme, S., Prowatke, S., Hametner, K., Gunther, D., 2005. Partitioning of trace elements between rutile and silicate melts: implications for subduction zones. Geochim. Cosmochim. Acta 69, 2361–2371. https://doi.org/10.1016/j.gca.2004.11.015.

Kontinen, A., 1987. An early proterozoic ophiolite - the jormua mafic-ultramafic complex, Northeastern Finland. Precambrian Res. 35, 313–341. https://doi.org/10.1016/0301-9268(87)90061-1.

Košler, J., Sláma, J., Belousova, E., Corfu, F., Gehrels, G.E., Gerdes, A., Horstwood, M.S. A., Sircombe, K.N., Sylvester, P.J., Tiepolo, M., 2013. U-Pb detrital zircon analysis–Results of an inter-laboratory comparison. Geostand. Geoanalytical Res. 37, 243–259.

Kusky, T.M., Li, J., Tucker, R.D., 2001. The archean dongwanzi oceanic crust and mantle. Science 80, 1142–1146.

Martin, C., Flores, K.E., Harlow, G.E., 2016. Boron isotopic discrimination for subduction-related serpentinites. Geology 44, 899–902. https://doi.org/10.1130/G38102.1.

McDonough, W.F., Sun, S. s., 1995. The composition of the Earth. Chem. Geol. 120, 223–253. https://doi.org/10.1016/0009-2541(94)00140-4.

Medaris, L.G., Singer, B.S., Jicha, B.R., Malone, D.H., Schwartz, J.J., Stewart, E.K., Van Lankvelt, A., Williams, M.L., Reiners, P.W., 2021. Early Mesoproterozoic evolution of midcontinental Laurentia: Defining the geon 14 Baraboo orogeny. Geosci. Front. 12, 101174 https://doi.org/10.1016/j.gsf.2021.101174.

Moores, E.M., 2002. Pre-1 Ga (pre-Rodinian) ophiolites: Their tectonic and environmental implications. Bull. Geol. Soc. Am. 114, 80–95. https://doi.org/10.1130/0016-7606(2002)114<0080:PGPROT>2.0.CO;2.

O'Driscoll, B., Walker, R.J., Day, J.M.D., Ash, R.D., Stephen Daly, J., 2015. Generations of melt extraction, melt-rock interaction and high-temperature metasomatism preserved in peridotites of the ~497 Ma Leka Ophiolite Complex, Norway. J. Petrol. 56, 1797–1828. https://doi.org/10.1093/petrology/egv055.

Paces, J.B., Miller Jr, J.D., 1993. Precise U-Pb ages of Duluth complex and related mafic intrusions, northeastern Minnesota: Geochronological insights to physical, petrogenetic, paleomagnetic, and tectonomagmatic processes associated with the 1.1 Ga midcontinent rift system. J. Geophys. Res. Solid Earth 98, 13997–14013.

Pagé, P., Bédard, J.H., Tremblay, A., 2009. Geochemical variations in a depleted fore-arc mantle: The Ordovician Thetford Mines Ophiolite. Lithos 113, 21–47. https://doi.org/10.1016/j.lithos.2009.03.030.
Paton, C., Hellstrom, J., Paul, B., Woodhead, J., Hergt, J., 2011. Iolite: Freeware for the visualisation and processing of mass spectrometric data. J. Anal. Spectrom. 26, 2508–2518.
Pearce, J.A., Reagan, M.K., 2019. Identification, classification, and interpretation of boninites from Anthropocene to Eoarchean using Si-Mg-Ti systematics. Geosphere 15, 1008–1037. https://doi.org/10.1130/GES01661.1.
Peltonen, P., Kontinen, A., Huhma, H., 1996. Petrology and Geochemistry of Metabasalts from the 1.95 Ga Jormua. J. Petrol. 37, 1359–1383.
Pe-Piper, G., Tsikouras, B., Hatzipanagiotou, K., 2004. Evolution of boninites and island-arc tholeiites in the Pindos Ophiolite. Greece. Geol. Mag. 141, 455–469. https://doi.org/10.1017/S0016756804009215.
Reagan, M.K., Pearce, J.A., Petronotis, K., Almeev, R.R., Avery, A.J., Carvallo, C., Chapman, T., Christeson, G.L., Ferré, E.C., Godard, M., 2017. Subduction initiation and ophiolite crust: new insights from IODP drilling. Int. Geol. Rev. 59, 1439–1450.
Saccani, E., Photiades, A., 2004. Mid-ocean ridge and supra-subduction affinities in the Pindos ophiolites (Greece): implications for magma genesis in a forearc setting. Lithos 73, 229–253. https://doi.org/10.1016/j.lithos.2003.12.002.
Schneider, D.A., Holm, D.K., O Boyle, C., Hamilton, M., Jercinovic, M., Whitney, D.L., Teyssier, C., Siddoway, C.S., 2004. Paleoproterozoic development of a gneiss dome corridor in the southern Lake Superior region, USA. Spec. Pap. Soc. Am. 339–358.
Schoene, B., Crowley, J.L., Condon, D.J., Schmitz, M.D., Bowring, S.A., 2006. Reassessing the uranium decay constants for geochronology using ID-TIMS U-Pb data. Geochim. Cosmochim. Acta 70, 426–445.
Schulz, K.J., Ayuso, R.A., 1998. Crustal recyling in the evolution of the Penokean orogen, in: Isotopic Evidence for Archean Contributions to Crustal Growth in the Pembine-Wausau Terrane, Northern Wisconsin, Institute on Lake Superior Geology, Part 1: Program and Abstracts. pp. 113–114.
Schulz, K.J., LaBerge, G.L., 2003. Trip 1. Pembine-Wausau magmatic terrane. Institute on Lake Superior Geology, Proceedings, v. 49, Part 2, 33-46.
Schulz, K.J., Cannon, W.F., 2007. The Penokean orogeny in the Lake Superior region. Precambrian Res. 157, 4–25. https://doi.org/10.1016/j.precamres.2007.02.022.
Scott, D.J., Helmstaedt, H., Bickle, M.J., 1992. Purtuniq ophiolite, Cape Smith belt, northern Quebec, Canada: A reconstructed section of early Proterozoic oceanic crust. Geology 20, 173–176. https://doi.org/10.1130/0091-7613(1992)020<0173:POCSBN>2.3.CO;2.
Scott, D.J., St-Onge, M.R., Lucas, S.B., Helmstaedt, H., 1999. The 2.00 Ga purtuniq ophiolite, Cape Smith Belt, Canada: Morb-like crust intruded by OIB-like magmatism. Ofioliti 24, 199–215.
Sims, P.K., Schulz, K.J., 1993. Geologic map of Precambrian rocks of parts of Iron Mountain and Escanaba 30' x 60' Quadrangles, Northeastern Wisconsin and adjacent Michigan. USGS Misc. Investig. Ser. Map 1–2356.
Sims, P.K., Van Schmus, W.R., Schulz, K.J., Peterman, Z.E., 1989. Tectono-stratigraphic evolution of the Early Proterozoic Wisconsin magmatic terranes of the Penokean Orogen. Can. J. Earth Sci. 26, 2145–2158.
Sims, P.K., 1992. Geologic map of Precambrian rocks, southern Lake Superior region, Wisconsin and northern Michigan.
Sláma, J., Košler, J., Condon, D.J., Crowley, J.L., Gerdes, A., Hanchar, J.M., Horstwood, M.S.A., Morris, G.A., Nasdala, L., Norberg, N., 2008. Plešovice zircon—a new natural reference material for U-Pb and Hf isotopic microanalysis. Chem. Geol. 249, 1–35.
Steinmann, G., Dilek, Y., Newcomb, S., 1927. Die ophiolitshen zonen in den mediterranen Kettengebirgen, translanted and reprinted by Bernoulli and Friedman. Dilek Newcom. Ed. Ophiolite Concept Evol. Geol. Thought, Geol. Soc. Am. Spec. Publ. 373, 77–91.
Stern, R.J., 2005. Evidence from ophiolites, blueschists, and ultrahigh-pressure metamorphic terranes that the modern episode of subduction tectonics began in Neoproterozoic time. Geology 33, 557–560. https://doi.org/10.1007/978-3-642-40994-3_23.
Stern, R.J., Reagan, M., Ishizuka, O., Ohara, Y., Whattam, S., 2012. To understand subduction initiation, study forearc crust: To understand forearc crust, study ophiolites. Lithosphere 4, 469–483. https://doi.org/10.1130/L183.1.
Stern, R.A., Syme, E.C., Lucas, S.B., 1995. Geochemistry of 1.9 Ga MORB- and OIB-like basalts from the Amisk collage, Flin Flon Belt, Canada: Evidence for an intra-oceanic origin. Geochim. Cosmochim. Acta 59, 3131–3154. https://doi.org/10.1016/0016-7037(95)00202-B.
Stern, R.J., 2020. The Mesoproterozoic Single-Lid Tectonic Episode: Prelude to Modern Plate Tectonics. GSA Today 30, 4–10. https://doi.org/https://doi.org/10.1130/GSATG480A.1.
Stern, R.J., 2023. The Orosirian (1800-2050 Ma) plate tectonic episode: Key for reconstructing the Proterozoic tectonic record. Geosci. Front. 101553.
Sun, S. -s., McDonough, W.F., 1989. Chemical and isotopic systematics of oceanic basalts: implications for mantle composition and processes. Geol. Soc. London, Spec. Publ. 42, 313–345. .
Tang, M., Chen, K., Rudnick, R.L., 2016. Archean upper crust transition from mafic to felsic marks the onset of plate tectonics. Science 80). 351, 372–375.
Van Schmus, W.R., 1976. Early and Middle Proterozoic History of the Great Lakes Area, North America. Philos. Transl. r. Soc. London A 280, 605–628.
Van Wyck, N., Johnson, C.M., 1997. Common lead, Sm-Nd, and U-Pb constraints on petrogenesis, crustal architecture, and tectonic setting of the Penokean orogeny (Paleoproterozoic) in Wisconsin. Bull. Geol. Soc. Am. 109, 799–808. https://doi.org/10.1130/0016-7606(1997)109<0799:CLSNAU>2.3.CO;2.
Vermeesch, P., 2018. IsoplotR: A free and open toolbox for geochronology. Geosci. Front. 9, 1479–1493.
Wakabayashi, J., Dilek, Y., 2004. What constitutes "emplacement" of an ophiolite?: Mechanisms and relationship to subduction initiation and formation of metamorphic soles. Geol. Soc. Spec. Publ. 218, 427–447. https://doi.org/10.1144/GSL.SP.2003.218.01.22.
Whattam, S.A., Stern, R.J., 2011. The "subduction initiation rule": A key for linking ophiolites, intra-oceanic forearcs, and subduction initiation. Contrib. to Mineral. Petrol. 162, 1031–1045. https://doi.org/10.1007/s00410-011-0638-z.
Wiedenbeck, M., Alle, P., Corfu, F.Y., Griffin, W.L., Meier, M., Oberli, F. v, Quadt, A. von, Roddick, J.C., Spiegel, W., 1995. Three natural zircon standards for U-Th-Pb, Lu-Hf, trace element and REE analyses. Geostand. Newsl. 19, 1–23.
Yellappa, T., Santosh, M., Chetty, T.R.K., Kwon, S., Park, C., Nagesh, P., Mohanty, D.P., Venkatasivappa, V., 2012. A Neoarchean dismembered ophiolite complex from southern India: Geochemical and geochronological constraints on its suprasubduction origin. Gondwana Res. 21, 246–265. https://doi.org/10.1016/j.gr.2011.05.003.
Zi, J.W., Sheppard, S., Muhling, J.R., Rasmussen, B., 2022. Refining the Paleoproterozoic tectonothermal history of the Penokean Orogen: New U-Pb age constraints from the Pembine-Wausau terrane, Wisconsin, USA. Bull. Geol. Soc. Am. 134, 776–790. https://doi.org/10.1130/B36114.1.